INVESTIGATION OF THE MODIFIED DOBSON'S METHOD AND PROPOSAL FOR IMPROVEMENT

MASTER REPORT MECHANICAL ENGINEERING

J.B. JOSSO

DYNAMICS BASED MAINTENANCE,
FACULTY OF ENGINEERING TECHNOLOGY,
UNIVERSITY OF TWENTE

April 25, 2025

Backside of the title page

Contents

Summary

This thesis investigates the Modified Dobson's method. This method for nonlinear system identification works well when the system's eigenmodes are far apart in frequency. However, when two modes are close together, the method lacks accuracy in the modal parameters that it generates. To better understand this, a computational model of the Modified Dobson's method was made and first used on linear systems. Modes that are in closer proximity to the mode of interest resulted in increased inaccuracy of the modal parameters. To improve this method, the shape of the resonance of a nearby mode was estimated and subtracted from the total system's response. This Improved Modified Dobson's method performed better than the original method. The modal parameters that were generated were more accurate. These improvements are expected to work partly for nonlinear systems, where the Modified Dobson's method was created for.

List of Symbols

$\alpha(\omega)$	receptance
$\ddot{x}$	acceleration
δ	modal constant magnitude ratio
η	damping loss factor
γ	damping ratio
Λ	function within the Dobson's method
ν_{abs}	maximum IMC value
ν_{phase}	maximum IPC value
Ω	frequency
ω	frequency
ω_0^{fxr}	left fixer frequency
ω_i^{swp}	sweeper frequency
ω_r	eigenfrequency
ω_{N+1}^{fxr}	right fixer frequency
$\overline{X}$	complex amplitude response
ϕ_r	angle of modulus of the modal constants
a	eigenfrequency ratio
A_r	real part of modal constant
B_r	imaginary part of the modal constant
c_I	Dobson's procedure parameter
C_r	modulus of the modal constants
c_R	Dobson's procedure parameter
d	hysteretic damping coefficient
d_I	Dobson parameter
d_R	Dobson parameter
F	excitation force amplitude
f	force
k	stiffness
m	mass
m_I	line-fit parameter
m_R	line-fit parameter

N	number
n_I	line-fit parameter
n_R	line-fit parameter
$R(\omega)$	residual receptance
t	time
t_I	Dobson's procedure parameter
t_R	Dobson's procedure parameter
u_I	Dobson parameter
u_R	Dobson parameter
x	amplitude

1 Introduction

1.1 Aim of this research

Eigenfrequencies are everywhere, from the tuning fork at singing class to your washing machine that starts shaking when it is rotating at exactly the right frequency. The resonance that occurs at the eigenfrequency can cause damage, as the reduced damping at resonance makes the object vibrate with much higher amplitudes than at other frequencies. Sticking to the washing machine, it passes through a large range of frequencies continuously, when going from full speed rotation back to a standstill. At one of these frequencies, the machine can shake heavily; however, the resulting damage is limited, because the shaking only lasts for a brief moment in time. This would be different when the eigenfrequency matches the operating frequency of the machine, which would cause a lot of shaking of the machine, so large vibrations for a prolonged time and thus possible damage due to large deflections.

In general, it is thus important to know where the eigenfrequencies of any application are located, to ensure these are not the operating frequencies. By exciting a device or component at a range of frequencies, it is possible to measure the response to see where these eigenfrequencies are located. In the case of linear eigenfrequencies, these frequencies will not change for larger excitation forces and only a linearly increasing response is seen. For nonlinear eigenfrequencies, however, the eigenfrequencies could shift with a higher excitation force. This could result in an eigenfrequency at 500 Hz for low forces that shifts to 550 Hz for higher excitation forces. The result of this is that a larger frequency range should be avoided in the operating frequency and that it is thus important to know if an eigenfrequency is nonlinear.

Many types of nonlinear eigenmodes exist, but in general they have one thing in common: a doubling of the magnitude of the excitation force will not result in a doubling of the response, which does is the case for linear modes [1]. This response is thus not linearly related to the excitation. There is also the possibility that the principle of linear superposition does not apply, but this is outside the scope of this master's thesis.
One source of nonlinearity is Coulomb friction, also called dry friction, which will make the response nonlinearly dependent on the force that is applied. The resonance peak will remain symmetric in this case, but the height of it will increase with an increase in the force that is applied for creating the resonance curve.
Another source of nonlinearity is a cubic stiffness. This will make the resonance peak asymmetric, where it curves more for higher excitation forces. Cubic softening will result in the resonance curving to the left, while cubic hardening will result in the resonance curving to the right, which could also be caused by clearance in the system under investigation [2]. The curve of such a skewed resonance, as is the first resonance in Figure 1.1, can be visualised with a backbone curve. This makes it also possible to compare the amount of curve in the resonance for different force levels, as backbones can be compared more easily than the (partly) overlapping resonances in case Frequency Response Functions (FRF's) at multiple force levels are plotted on top of each other.

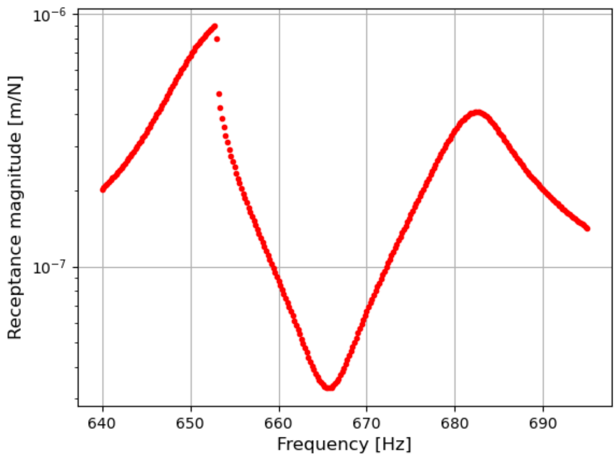

Figure 1.1: *Example of an FRF with multiple resonances of which the first is clearly a skewed resonance of a nonlinear eigenmode*

One of the methods to identify nonlinear eigenmodes is the Modified Dobson's method, that was developed by Di Maio [3]. It can create the backbone curve of a nonlinear resonance peak to show its curvature. The method originates from the '80s, as the so-called Dobson's method, which on its own is an expansion of the line-fit method. Although these methods for analysing linear eigenmodes are outdated by now, the Dobson's method possesses qualities that are of significance for nonlinear eigenmodes and resulted in the Modified Dobson's method.

The backbone curve is extracted accurately for a single isolated nonlinear resonance, as is described by Di Maio [3]. It was found that for multiple resonances, even if relatively far from each other, the Modified Dobson's method fails. Instead of a curved clear single line, the backbone starts splitting at the bottom, like a letter λ, as can be seen in Figure 1.2. In case of severe splitting, this makes the curve of a nonlinear resonance much harder to see from this backbone. Therefore, the splitting of the backbone had to be studied in more detail, to come up with possible solutions, that would make the analysis of close nonlinear resonances possible.

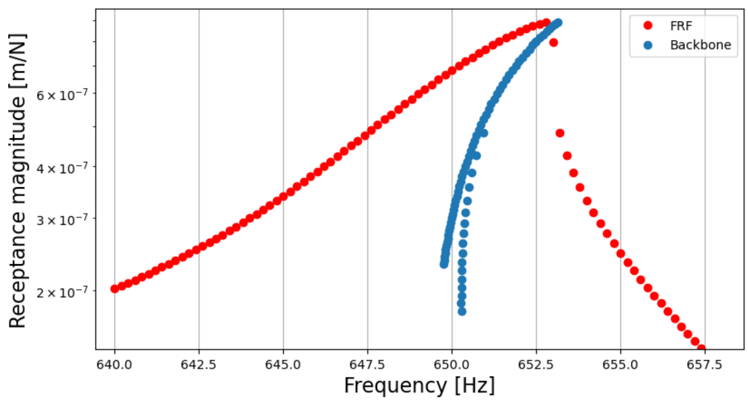

Figure 1.2: *Zoom-in on the first resonance of Figure 1.1 and the split backbone of this skewed resonance of a nonlinear eigenmode*

This gives the following research question:

What is the effect of an increasingly closer other mode on the Modified Dobson's analysis of the mode of interest and how can negative effects of a close mode be reduced, to improve the results of the Modified Dobson's method?

1.2 Outline

The outline of this thesis is as follows.

Chapter 2 gives a literature review about experimental methods and methods for the identification of nonlinear eigenfrequencies, such as the Modified Dobson's method.

Chapter 3 describes the theoretical background of eigenfrequencies and how to plot them. Besides this, linear identification methods are introduced, like the previously discussed line-fit method and the Dobson method, that can be used to extract information about the eigenfrequencies.

Chapter 4 subsequently discusses the Modified Dobson's method, which was inspired by the other methods, but can be used to analyse nonlinear eigenfrequencies. The problems that arise for close other modes are described and analysed for linear eigenfrequencies, to stick to the core of the problem, which is the splitting of the backbone.

Chapter 5 provides a possible solution to the splitting of the backbone. This is again tested for linear eigenfrequencies, to be able to check the effect without disturbance of the curve in the backbone coming from any nonlinear eigenfrequency. Besides this, the link is made to nonlinear eigenfrequencies. For the Modified Dobson's method [3], a comparison between the results of the computational model in Python that was created during this thesis and the results of the computational model of Di Maio is made to include some checks-and-balances.

Chapter 6 concludes this thesis work and gives recommendations for future research.

2 Literature review

Modal analysis is a technique to analyse the dynamics of a linear system, which has been used for decades. The analysis results in a mathematical response model of the system, consisting of its eigenfrequencies, damping ratios and modal constants (mode shapes). The discipline of modal analysis has been researched extensively by, among others, Maia and Silva [4] and Ewins [1]. In order to discuss the recent state of literature regarding modal analysis, a brief explanation of the fundamental concepts for linear systems will be given in the next paragraph.

The experimental modal analysis of a linear system starts by making a Frequency Response Function (FRF), which is one of the most broadly used functions to characterise the dynamic behaviour of a system. After measuring a system, the FRF shows the ratio between the response and excitation as a function of excitation frequency. This ratio between response and excitation is called the receptance in case of displacement amplitude and force amplitude respectively. Subsequently, the modal analysis can be performed on this FRF. This will identify the modal parameters of the FRF, which are the aforementioned eigenfrequencies, damping ratios and modal constants. Then, these modal parameters can be used to regenerate or synthesise the measured FRF with a mathematical response model, which can subsequently be compared with the measured FRF, to make sure that the modal parameters that are found are reliable. This regeneration-check of the modal parameters ensures a sturdy identification of a linear system using experimental modal analysis.

In case of nonlinear systems, other techniques are required, as the standard modal analysis techniques for linear systems do not work. This failure is caused by the regeneration-check that fails for nonlinear systems, since the FRF is not a function of just the frequency in that case. Nayfeh and Mook [5] and Worden and Tomlinson [2] have shown that the response of a nonlinear system is generally a function of excitation frequency and the force of the excitation. This means that the FRFs can look different for a low and for a high force level. A nonlinear system can therefore better be characterised with a Frequency Response Curve (FRC) compared to a FRF.
Multiple types of 3D surface representations to visualise the FRC of a nonlinear system are introduced. Karaağaçlı and Özgüven [6] described a Harmonic Force Surface (HFS) which is a surface defined in the space spanned by frequency, displacement amplitude and force amplitude. Figure (2.1) gives an example of an HFS, visualising that multiple FRFs, showing the receptance as function of frequency, are possible. It can clearly be seen that this receptance is not constant for a frequency of, for instance, 12 Hz and that the FRFs would thus look different for low and high force levels.

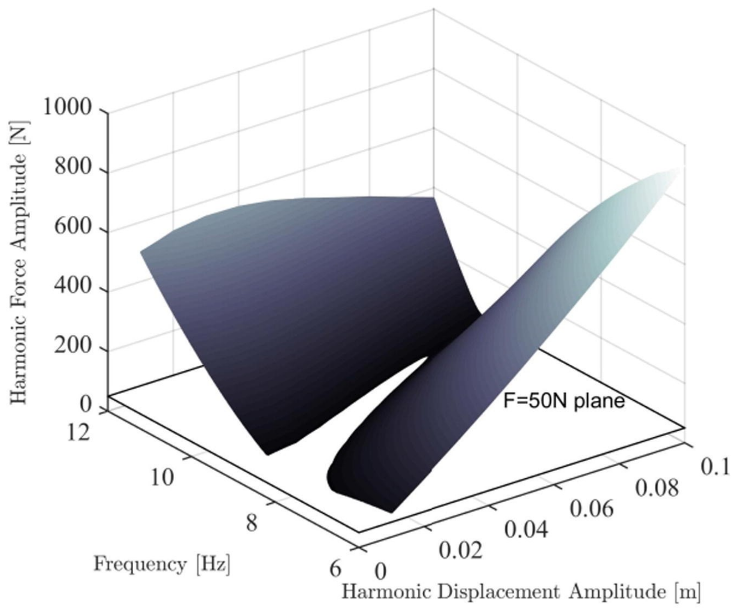

Figure 2.1: *Example of a harmonic force surface of a nonlinear system, adapted from [6]*

.

The HFS is created by Response-Controlled Testing (RCT) in which the displacement amplitude is kept constant, which is done for multiple amplitude levels. Abeloos et al. [7] on the other hand, proposed a response surface in a space slightly different than that of the HFS, as here, it is spanned by the maximum of the displacement amplitude, instead of amplitude itself. Like the HFS, there is the Forced Response Surface (FRS) which was introduced by Li et al. [8]. The FRS can be seen as a group of constant-force FRCs. Di Maio [3] proposed a Nonlinear Frequency Response Surface (NFRS), which can be used to characterise the dynamics of a nonlinear system in a steady-state situation. The hypothesis of the NFRS is that linear response models are able to model a nonlinear system, by forming a large array of linear FRFs, in which each FRF has a different response amplitude, creating an NFRS that represents a nonlinear system. An example of an NFRS can be seen in Figure (2.2), where the top view in Figure (2.2 b) clearly shows that the receptance (Amplitude X/F) is not just a function of frequency, but also of displacement. For a higher displacement response, which is related to a higher exciting force, the maximum receptance shifts in frequency. This shows that this system is nonlinear as it is a function of both excitation frequency and the force of the excitation. The use of linear FRFs within NFRS makes it a more intuitive approach for analysing nonlinear systems for practitioners that are used to linear FRF analysis compared to many other techniques to analyse nonlinear systems.

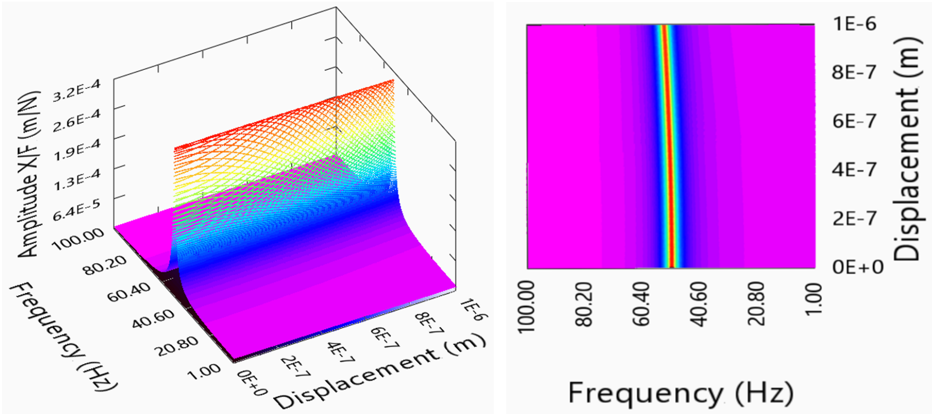

(a) *Perspective view of the NFRS*

(b) *Top view of the NFRS*

Figure 2.2: *Example of a nonlinear frequency response surface, adapted from [3]*
.

In the last 15 years, experimental methods have been developed that identify the modal parameters of a nonlinear system directly, using phase resonance testing of Nonlinear Normal Modes (NNMs). An NNM is defined as a periodic synchronous vibration of a nonlinear system and was investigated as one of the first by Rosenberg [9] in 1966. The phase resonance criterion was generalised to nonlinear systems by Peeters et al. [10], enabling using it to excite a single NNM. After achieving phase resonance, the modal parameters that depend on the amplitude can be identified using time-frequency methods. The phase resonance could be achieved automatically using a Phase-Locked Loop (PLL) and an adaptive filter, Peter and Leine [11] proposed. With a PLL, it is possible to draw the backbone of a NNM by experimental continuation over the response amplitude. Likewise, Renson et al. [12] developed Control-Based Continuation (CBC) to execute fixed-frequency tests, which can be used to draw the S-curves of nonlinear systems by experimental continuation over the response amplitude. Adaptive filtering was proposed by Abeloos et al. [7] to cancel the CBC controller's invasiveness to the dynamics of the tested system.

Karaağaçlı and Özgüven [6, 13, 14] proposed the previously discussed RCT method, which can be seen as an alternative to the CBC and PLL methods, in which experimental continuation over the excitation frequency is executed, while keeping the response amplitude constant. These new methods reduced the time needed for analysis, but they do require refined testing setups that use specially designed controllers. Another testing method was developed by Zhang et al. [15, 16, 17] which works like the fixed-frequency CBC, but now the excitation voltage is used as the experimental continuation parameter. This removes the need for closed-loop controllers, which makes the experiments significantly easier.

Besides the experimental methods, there are identification methods like the CONCERTO method by Carrella and Ewins [18, 19], dating from 2011. It identifies a corresponding linear system that fits the measured nonlinear response for each response amplitude. It was based on the PhD thesis of Lin [20] and the book of Maia and Silva [4]. The CONCERTO method has the advantage of easy implementation, but it can only be used on isolated modes as it assumes a single degree of freedom (SDOF) system. Besides this, the method fails to perform accurately in case of discontinuities in the FRC that is measured.

Recently, a new method for nonlinear system identification was introduced: the Modified Dobon's method. It was developed by Di Maio [3] and is based on the

Dobson line-fit method [21] for linear systems, from the 80's. With the modification, it becomes possible to also analyse nonlinear systems. Using the NFRS introduced earlier, it is possible to identify nonlinear modal parameters from just one FRC. Like in the method from Zhang [15, 16, 17], the modified Dobson method does not require to control the amplitude of the force or the response, which leaves more time for analysing instead of testing. The Modified Dobson's identification method [3] is used to investigate nonlinear systems in the frequency domain under steady-state conditions, which makes it differ from, for instance, the experimental method of Renson [12] that was designed for nonlinear vibrations, that are not steady-state.

Like the identification method of CONCERTO [18, 19], the Modified Dobon's method is only suited for well-separated modes [3]. The effect of the distance between modes on the accuracy of the Modified Dobson's method is an important topic in this thesis and will be investigated in detail. Chapter 3.2.1 of the PhD thesis of Maia [22] about "Interference criteria" could be of use here, as it helps to quantify the influence of one mode on the other, which is related to the distance between the two. Subsequently, a solution to the problems close modes create for the Modified Dobson's method is sought and described within this thesis. In the future, the paper of Maia [23] about the Global Dobson's method, which incorporates multiple FRFs, could be of use to extend the Modified Dobson method from single input single output (SISO) to single input multiple output (SIMO) experiments, for which a first step is described in Appendix A.6.

3 Theoretical background

This chapter gives the theoretical background for this thesis. First, the term receptance is introduced and explained in Chapter 3.1. Then the different ways of plotting this receptance are discussed in Chapter 3.2. Subsequently, Chapter 3.3 describes the differences between SDOF and MDOF receptance models. Chapter 3.4 discussed different identification methods that lay at the basis of the Modified Dobson's method. At the end, Chapter 3.5 give the interference criteria that could be used to qualify the proximity of eigenfrequencies to each other.

3.1 Receptance

Different damping formulations exist, the viscous damping force depends on the velocity of a system, while the hysteretic damping force depends on the amplitude of a system. Both are used to model energy dissipation, but for the viscous damping this dissipation is frequency dependent, where many materials and structures show behaviour that is closer to frequency independent energy dissipation [4]. In this thesis, there is thus focused on hysteretic damping, also called structural damping, which is frequency independent. The equation of motion of a hysteretically damped linear system is

$$m\ddot{x}(t) + (k + id)x(t) = f(t), \tag{3.1}$$

in which x is the amplitude of the system in meter, $\ddot{x}$ is the acceleration of the system in m/s^2, m is the mass of the system in kg, k is the stiffness and d is the hysteretic damping coefficient, both in N/m, i is the imaginary unit, f is the force that is being applied to the system in Newton and t is the time in seconds [24].
Using some trial solutions the equation of motion could be rewritten to

$$(-\omega^2 m + k + id)\overline{X}e^{i\omega t} = Fe^{i\omega t}, \tag{3.2}$$

where ω is the frequency in rad/s, $\overline{X}$ is the complex amplitude response of the system in meter, which allows for a phase angle between the response and the forcing, and F is the harmonic excitation force amplitude in Newton acting on the system [4].

The Frequency Response Function (FRF) is the ratio between response and excitation as a function of the frequency. The receptance $\alpha(\omega)$ is a possible form of FRF and is a complex function of the eigenfrequencies, or so-called resonances, that are present in the system that is measured. This $\alpha(\omega)$ in m/N can be calculated using

$$\alpha(\omega) = \frac{\overline{X}(\omega)}{F(\omega)}. \tag{3.3}$$

With the analysis of a measured receptance, $\alpha(\omega)$, it is therefore possible to make an estimation of the displacement response of the system for when a force with a certain frequency is applied to the system. This makes the FRF a valuable measurement, as it shows at which frequencies the resonances are located and whether they show a small or large response.

Combining Equation (3.2) and (3.3) gives that the receptance $\alpha(\omega)$ of a single degree of freedom (SDOF) linear system with structural damping can be described theoretically with

$$\alpha(\omega) = \frac{1}{(k - \omega^2 m) + id}. \tag{3.4}$$

The properties k, m and d of the SDOF linear system can be used to calculate the eigenfrequency ω_r in rad/s with

$$\omega_r = \sqrt{\frac{k}{m}}, \tag{3.5}$$

and to calculate the dimensionless structural damping loss factor η with

$$\eta = \frac{d}{k}. \tag{3.6}$$

The subscript r in Equation 3.5 stands for resonance, which will occur at the eigenfrequency of a (undamped) system.

3.2 Plotting the receptance

As the receptance $\alpha(\omega)$ in Equation (3.4) is a complex function, containing a real and an imaginary part, plotting it over the frequency ω would result in a 3D-plot, which can be seen in Figure 3.1. Such plots are hard to read, especially when the projections that are present here would be missing. The projections on their own are a way to make reading the plots less hard.

3.2.1 Nyquist plot

One of these projections or plots is the Nyquist plot, as can be seen in the blue dotted projection in Figure 3.1. Using Nyquist, one plots the real value of a complex number on the horizontal axis and the imaginary value of a complex number on the vertical axis. The numerator and denominator of Equation (3.4) could be multiplied by the complex conjugate of the denominator, resulting in

$$\alpha(\omega) = \frac{(k - \omega^2 m) - id}{(k - \omega^2 m)^2 + d^2} = \frac{k - \omega^2 m}{(k - \omega^2 m)^2 + d^2} - i\frac{d}{(k - \omega^2 m)^2 + d^2}, \tag{3.7}$$

which an be used to split the receptance $\alpha(\omega)$ into a real and imaginary part to construct the Nyquist plot. The advantage of this is that the complexity of a receptance datapoint is seen immediately, the downside, however, is that the frequency values cannot be seen that easily. The frequency value of each datapoint, which are located at each nook of the FRF-curve in Figure 3.1, could be plotted as a number next to it. That would be sufficient to see the eigenfrequency in this example, but for multiple eigenfrequencies, displaying these frequency values in one single plane can get rather chaotic. For an SDOF linear system the Nyquist is less chaotic, see Figure 3.1, and it will show a circle with a radius of $\frac{1}{2d}$ [4], see Appendix A.1.

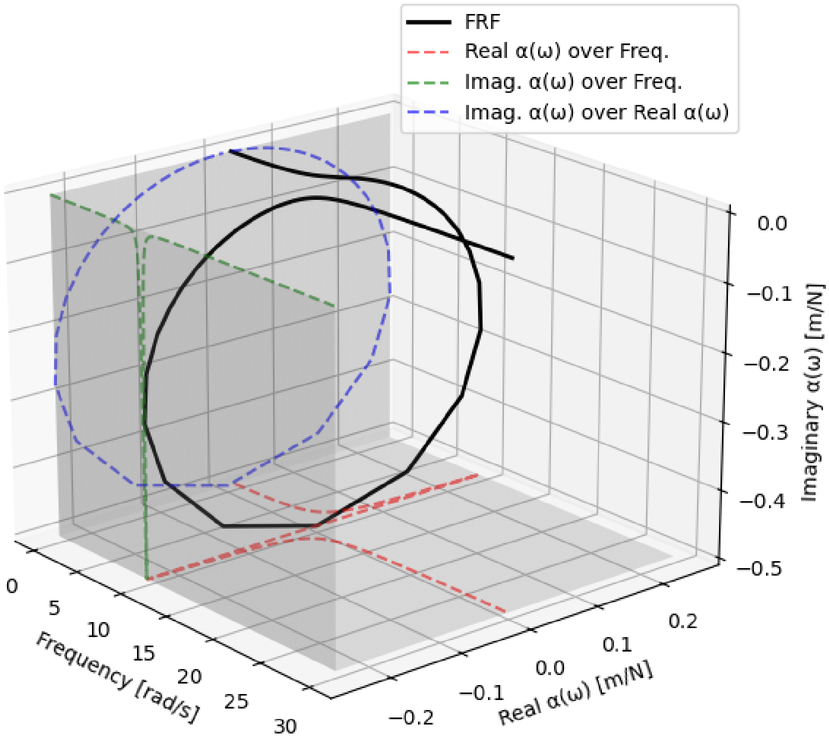

Figure 3.1: *Example of a 3D-plot including projections of the complex SDOF receptance $\alpha(\omega)$ with an eigenfrequency at 10 rad/s*

3.2.2 Separate real and imaginary plot

With multiple eigenfrequencies, plotting the real and imaginary parts of the receptance separately could be a clear way to display those. An example of this way of plotting, although for only one eigenfrequency, are the red and green projections in Figure 3.1. A disadvantage is that one has to take a look at two plots to get the full picture of the complexity of the receptance, without one plot that tells much more about the resonance frequencies.

3.2.3 Bode plot

A Bode plot also consists of two separate plots, but it is a little easier to grasp than a separate real and imaginary plot. A Bode plot consists of a magnitude plot and a phase plot, of which the former is the most important to look at in the field of modal analysis, as it clearly shows the eigenfrequency locations combined with an indication of the amount of damping of a certain resonance. For a more in-depth understanding of certain eigenfrequency (combinations) the phase part of the Bode plot could be investigated. The definition of magnitude is the distance from the origin in the Nyquist plot to a certain datapoint in that plot, so $|\alpha(\omega)|$. The phase is defined as the angle between an arrow from the origin to a datapoint in the Nyquist and the positive real axis. An example of a Bode plot is shown in Figure 3.2.

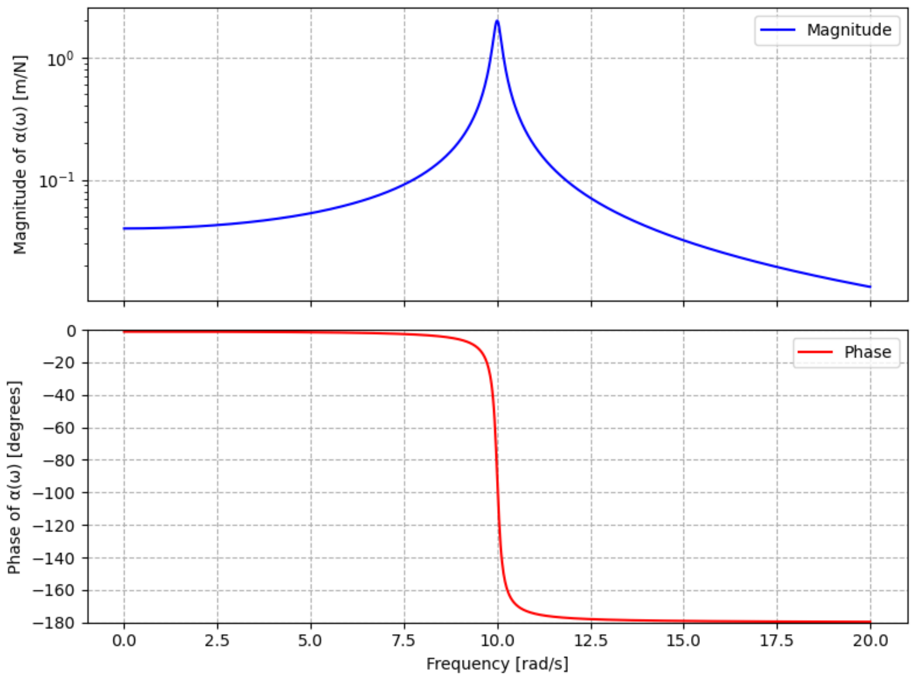

Figure 3.2: *Example of the magnitude (top) and phase (bottom) parts of the Bode plot of the complex receptance $\alpha(\omega)$ with an eigenfrequency at 10 rad/s*

3.3 SDOF versus MDOF

In case a system is modelled using an SDOF receptance model, its vibratory motion can only be described with one single coordinate [4]. To describe a mode shape, more coordinates are needed and an SDOF model would thus not suffice in that case. Then, a multiple degrees of freedom (MDOF) receptance model is needed, in which the number of the degrees of freedom is equal to the number of independent coordinates of the model. The FRF of an MDOF linear system will show multiple resonances or eigenfrequencies, which each have their own mode shape. This could be better understood with the equation for the total FRF response of a MDOF linear system. This is

$$\text{total-FRF} = \sum_{r=1}^{N} \alpha_r(\omega) = \sum_{r=1}^{N} \frac{A_r + iB_r}{\omega_r^2 - \omega^2 + i\eta_r\omega_r^2}, \tag{3.8}$$

in which the total FRF response is the sum of all the different eigenmodes, with r the number of the mode or resonance, N the total number of modes, where A_r and B_r are the modal constants in 1/kg, which can be used to construct mode shapes and η_r is the (dimensionless) damping loss factor of that specific eigenmode [1].
From Equation (3.8) the step can be made to a receptance model of an MDOF linear system that could be approximated with an SDOF system, which is

$$\alpha(\omega) = \frac{A_r + iB_r}{\omega_r^2 - \omega^2 + i\eta_r\omega_r^2}, \tag{3.9}$$

and could also be written as

$$\alpha(\omega) = \frac{C_r e^{i\phi_r}}{\omega_r^2 - \omega^2 + i\eta_r\omega_r^2}, \tag{3.10}$$

in which C_r is the modulus of the modal constants in $1/\text{kg}$ and ϕ_r is the angle of the modulus [4].
For eigenfrequencies that are closely-spaced in the FRF, the resonances cannot be described with Equation (3.9) and (3.10), as the tail of one resonance affects the shape of the other resonance, see Figure 3.3. In case the eigenfrequencies are well-separated, the resonances of an MDOF linear system could each be treated as an isolated SDOF linear system and Equation (3.9) and (3.10) do hold. This (tiny) tail of receptance of another mode is called the residual and it influeneces the magnitude and shape of the resonance that is being investigated.

The receptance value of a single mode will decrease quickly for frequencies further away from the eigenfrequency, but in normal measurement situations (with finite frequency values) there will, mathematically, always be some residual from other modes in MDOF situations.

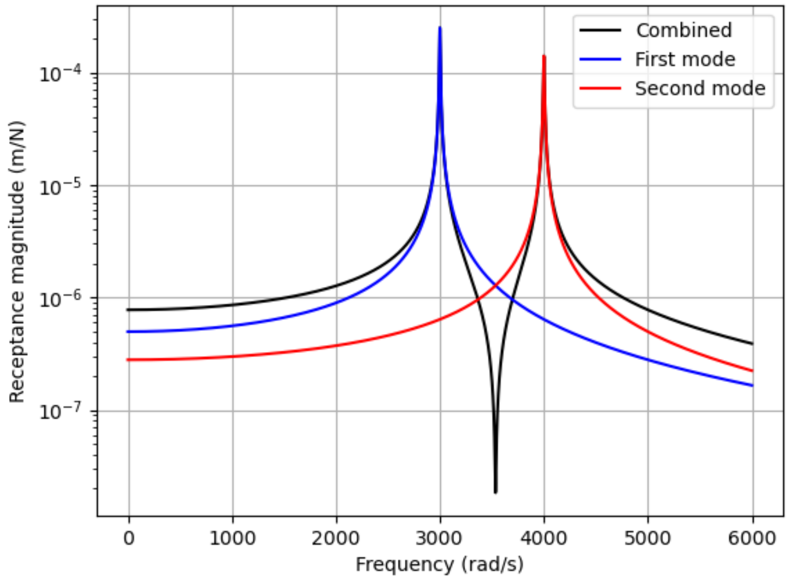

Figure 3.3: *Example of a magnitude-FRF with 2 resonances that are plotted separately and combined and thus a MDOF system, ω_1=3000 rad/s and ω_2=4000 rad/s*

3.4 Identification methods

With the measured receptance $\alpha(\omega)$ plotted with one or the other type of plot, one can move on to analysing it. This modal analysis is called the identification in which the properties like eigenfrequency, damping and the modal constants, as described in Equation (3.9) are calculated. These can subsequently be filled in into this equation to regenerate the receptance measurement to check their correctness. Several identification methods for modal analysis are described in this chapter.

3.4.1 Inverse-method

The inverse-method [4] is an analysis method more than an identification method, but it can be seen as a less sophisticated line-fit method of Chapter 3.4.2, hence that it is mentioned here. The inverse-method uses the inverse of the receptance $\alpha(\omega)$ of an SDOF linear system, as given in Equation (3.4). This makes that the inverse of the receptance is

$$\alpha(\omega)^{-1} = k - \omega^2 m + id, \tag{3.11}$$

where it becomes clear that the imaginary part of $\alpha(\omega)^{-1}$ is a constant, namely the hysteretic damping coefficient d. The real part of $\alpha(\omega)^{-1}$ is a linear function of ω^2, so plotting Re$(\alpha(\omega)^{-1})$ as a function of ω^2 would result in a line with a slope of $-m$ and an intercept of k. This can be written as

$$\text{Re}(\alpha(\omega)^{-1}) = k - m\omega^2, \tag{3.12}$$

and

$$\text{Im}(\alpha(\omega)^{-1}) = d. \tag{3.13}$$

With a measured FRF of real eigenfrequency in an SDOF linear system it is therefore relatively easy to determine the properties k, m and d of that system. Two plots are generated for this: a Re$(\alpha(\omega)^{-1})$ over ω^2 plot and an Im$(\alpha(\omega)^{-1})$ over ω^2 plot, although over ω would also be possible for Im$(\alpha(\omega)^{-1}$. In the Re$(\alpha(\omega)^{-1})$ plot a line is drawn to match the results as best around the eigenfrequency squared value. This line is expected to be not completely horizontal, as this would mean that the mass m of the system is zero. The stiffness k is subsequently determined by the point where the drawn line crosses the y-axis, the intercept. For the Im$(\alpha(\omega)^{-1})$ plot, also a line is drawn, but this time a horizontal one, as there is only an intercept value needed, which gives the hysteretic damping coefficient d.
With the properties k, m and d of the system determined, they can be checked by regenerating the FRF with Equation (3.4). This regenerated FRF should then reasonably match the measured FRF as a check for the correctness of the three determined properties.

3.4.2 Line-fit method

Slightly more complicated than the inverse-method is the line-fit identification method for modal analysis [25]. It also uses the inverse of the receptance α, to do two line-fits, hence its name. Again, one line-fit is done on the real part of the inverse of the receptance and one on the imaginary part, which are both plotted as a function of the frequency squared, see Figure 3.4 and 3.5. In this method however, the receptance is described with Equation (3.9) instead of Equation (3.4), so it holds for MDOF systems. The resonances of the MDOF system need to be separated that far, that the resonance that is analysed can be treated as a SDOF system, for Equation (3.9) to hold. When this is not the case, Equation (3.9) becomes

$$\alpha(\omega) = \frac{A_r + iB_r}{\omega_r^2 - \omega^2 + i\eta_r\omega_r^2} + R(\omega), \tag{3.14}$$

in which R in m/N is the residual receptance coming from other modes. For the line-fit method the residual is assumed to be zero, returning again to Equation (3.9). The equations for the fitted lines are therefore

$$\text{Re}(\alpha(\omega)^{-1}) = m_R + n_R\omega^2, \tag{3.15}$$

and

$$\text{Im}(\alpha(\omega)^{-1}) = m_I + n_I\omega^2, \tag{3.16}$$

where $\alpha(\omega)^{-1}$, m_R and m_I are in N/m=kg/s^2, n_R and n_I are in kg and ω is in rad/s. The line-fit parameters m_R and m_I are the initial values of the real and imaginary line-fit graphs respectively. The parameters n_R and n_I are the slopes of the real and imaginary line-fit graphs respectively.

For n_I is zero, the line-fit on $\text{Im}(\alpha(\omega)^{-1})$ gives a horizontal line. In this case, the line-fit method becomes equal to the inverse-method. Then, it will hold that $m_R = k$, $n_R = -m$ and $m_I = d$ and one can simply follow the inverse-method procedure, as it can be concluded that one is measuring an SDOF linear system and not an MDOF linear system that can be treated like SDOF.
For $n_I \neq 0$ the line-fit method is followed, the four line-fit parameters, described further in Appendix A.2, are then used to calculate the modal parameters of mode r with

$$\omega_r = \sqrt{\frac{-m_R n_R - m_I n_I}{n_R^2 + n_I^2}}, \tag{3.17}$$

$$\eta_r = \frac{m_R n_I - m_I n_R}{-m_R n_R - m_I n_I}, \tag{3.18}$$

$$A_r = \frac{-n_R}{n_R^2 + n_I^2}, \tag{3.19}$$

$$B_r = \frac{n_I}{n_R^2 + n_I^2}, \tag{3.20}$$

subsequently, these four modal parameters are used to regenerate the measured FRF using Equation (3.9). This way it can be checked if the regenerated receptance graph matches the measured receptance, which would indicate that the four modal parameters are determined correctly. An example of this can be seen in Figure 3.6, in which the line-fits were done using 11 datapoints, although this fit is rather poor. The line-fit method only works for modes with frequencies that are well spaced from each other [4].

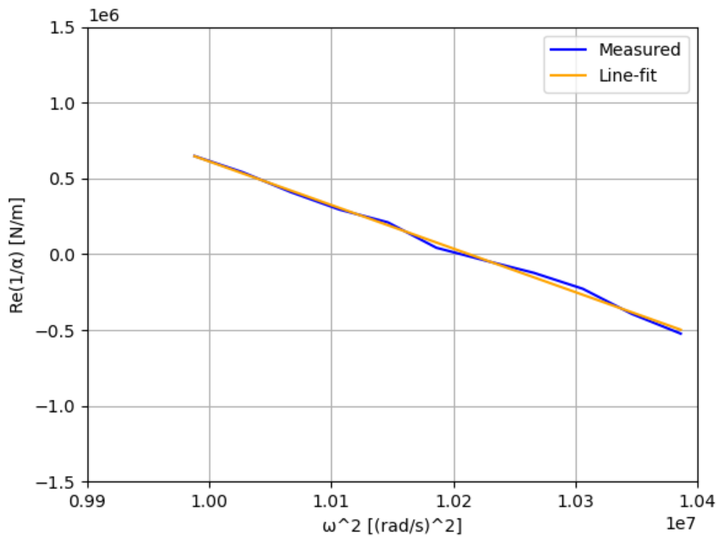

Figure 3.4: *Example to show the line-fit procedure on Re($\alpha(\omega)^{-1}$)*

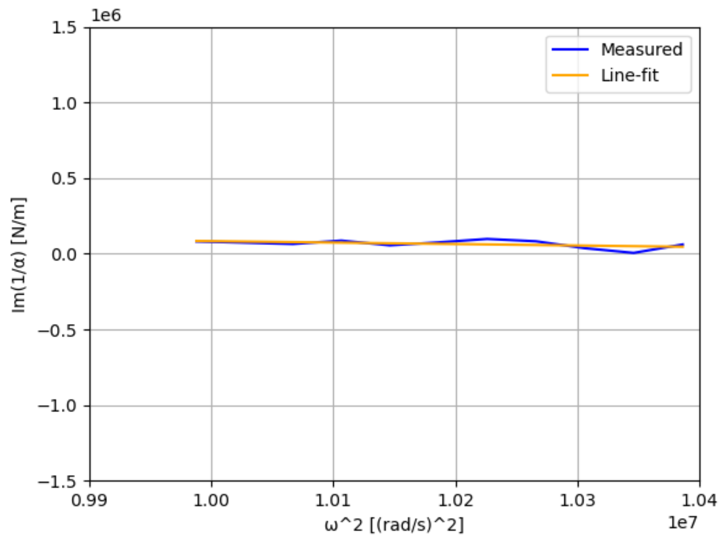

Figure 3.5: *Example to show the line-fit procedure on Im$(\alpha(\omega)^{-1})$*

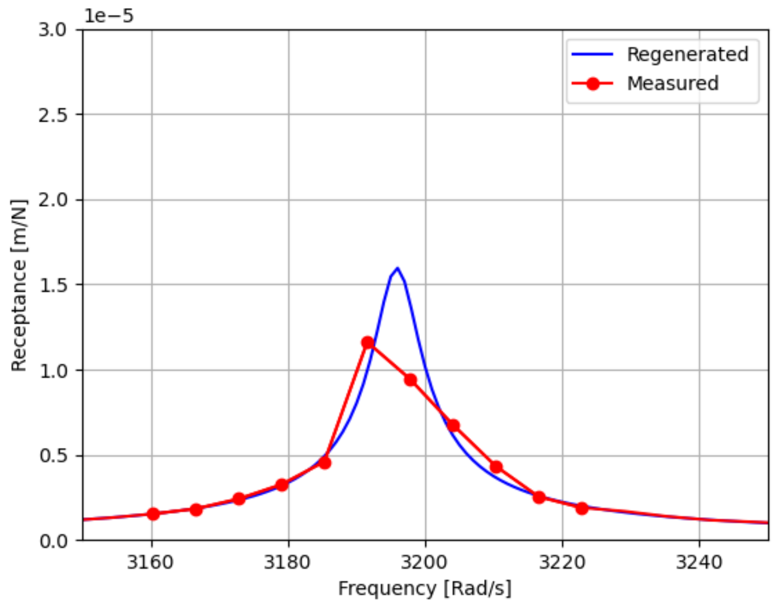

Figure 3.6: *Example of a regeneration using the line-fit method on 11 datapoints*

3.4.3 Dobson's method

The Dobson's method [21] could be seen as a more sophisticated line-fit method. It is less sensitive to a close mode, as it compensates for the effects of other modes up to a certain level. This is done by doing another line-fit on the results of a first round of multiple line-fits, which flattens disturbances like noise, but also other residuals from other modes, as the effect of outliers is small with these line-fits [4]. Equation (3.14) in which R, the residual receptance coming from other modes, is another way of writing the total receptance of an MDOF linear system in Equation (3.8). For an MDOF system with well-separated resonances, the residual R from other resonances can be assumed constant around the eigenfrequency of interest. This means that in Equation (3.14) R is a constant, for frequencies close to the eigenfrequency ω_r. Introducing a variable Ω which is a frequency in rad/s close to but not equal to the frequency ω in Equation (3.14) will then lead to

$$\alpha(\Omega) = \frac{A_r + iB_r}{\omega_r^2 - \Omega^2 + i\eta_r\omega_r^2} + R(\Omega). \tag{3.21}$$

Equation (3.14) and (3.21) can subsequently be subtracted to get rid of the residual-term R, resulting in

$$\alpha(\omega) - \alpha(\Omega) = (A_r + iB_r)[\frac{\omega^2 - \Omega^2}{(\omega_r^2 - \omega^2)(\omega_r^2 - \Omega^2) - \eta_r^2\omega_r^4 + i\eta_r\omega_r^2(2\omega_r^2 - \omega^2 - \Omega^2)}], \tag{3.22}$$

which only holds for an Ω that is sufficiently close to ω_r, as the residuals, written as $R(\omega)$ and $R(\Omega)$, can be approximated as equal then. A function Λ can be defined by dividing the term $\omega^2 - \Omega^2$ by Equation (3.22), this gives

$$\Lambda(\omega, \Omega) = \frac{\omega^2 - \Omega^2}{\alpha(\omega) - \alpha(\Omega)} = \frac{A_r - iB_r}{A_r^2 + B_r^2}[(\omega_r^2 - \omega^2)(\omega_r^2 - \Omega^2) - \eta_r^2\omega_r^4 + i\eta_r\omega_r^2(2\omega_r^2 - \omega^2 - \Omega^2)], \tag{3.23}$$

in which Λ is in kg/s^4. It is clear that Ω cannot be equal to ω, as it will result in dividing by zero. The function $\Lambda(\omega, \Omega)$ can be split into a real and imaginary part, like was done in the line-fit method in Chapter 3.4.2, giving

$$\mathrm{Re}(\Lambda) = c_R + t_R\omega^2, \tag{3.24}$$

and

$$\mathrm{Im}(\Lambda) = c_I + t_I\omega^2, \tag{3.25}$$

with the initial values c_R and c_I in kg/s^4 and the slopes t_R and t_I in kg/s^2=N/m. Equation (3.24) and (3.25) are linear functions when they are plotted as a function of ω^2, see the middle row in Figure 3.7. It can be proven from Equation (3.23) that the real and imaginary slopes, t_R and t_I respectively, can be written as

$$t_R = -\frac{1}{A_r^2 + B_r^2}[A_r(\omega_r^2 - \Omega^2) + B_r\eta_r\omega_r^2], \tag{3.26}$$

and

$$t_I = -\frac{1}{A_r^2 + B_r^2}[A_r\eta_r\omega_r^2 - B_r(\omega_r^2 - \Omega^2)]. \tag{3.27}$$

In Equation (3.26) and (3.27) it can be seen that they are also linear functions like Equation (3.24) and (3.25), but as functions of Ω^2 instead of ω^2. Equation (3.26) and (3.27) can thus be rewritten respectively as

$$t_R = d_R + u_R\Omega^2, \tag{3.28}$$

and

$$t_I = d_I + u_I\Omega^2. \tag{3.29}$$

In here d_R and d_I are in kg/s^2=N/m and u_R and u_I in kg. t_R and t_I are thus not constants, as they might look in Equation (3.24) and (3.25), but variables that depend on Ω^2, as can be seen from Equation (3.26) to (3.29).

In the Re(Λ) and Im(Λ) over ω^2 plots there are as such multiple lines plotted, each representing one Ω^2 value, see the middle row in Figure 3.7. The slope of each Ω^2-line, represented by t_R or t_I, can then be plotted as a function of Ω^2, see the bottom row in Figure 3.7. This is done for values of Ω^2 that are close to the eigenfrequency squared: ω_r^2.

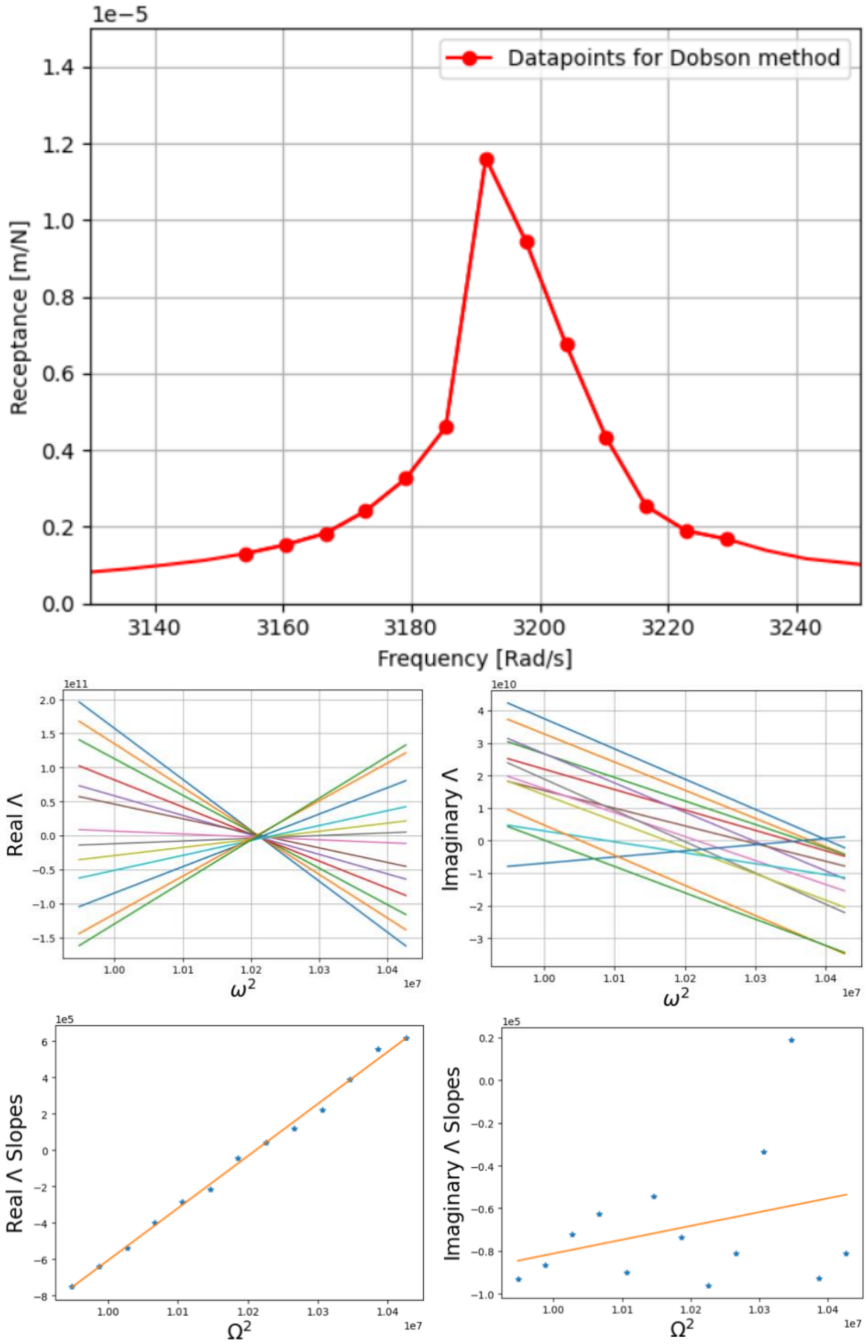

Figure 3.7: *Example Dobson procedure: top row: datapoints from the measured receptance, middle row: Λ plotted as function of ω^2 with each line representing one Ω^2-value related to one of the datapoints above, bottom row: slopes of each Ω^2-line plotted as function of this Ω^2.*

Plotting the t_R or t_I values as a function of Ω^2 will show a linear relationship, see the bottom row in Figure 3.7, although not so clear for the imaginary part for this experimental data, and Equation (3.28) and (3.29). The parameters from these equations can, using Equation (3.26) and (3.27), be rewritten to

$$d_R = -\frac{(A_r + B_r\eta_r)\omega_r^2}{A_r^2 + B_r^2}, \tag{3.30}$$

$$d_I = -\frac{(A_r\eta_r - B_r)\omega_r^2}{A_r^2 + B_r^2}, \tag{3.31}$$

$$u_R = \frac{A_r}{A_r^2 + B_r^2}, \tag{3.32}$$

$$u_I = -\frac{B_r}{A_r^2 + B_r^2}. \tag{3.33}$$

Equation (3.30) to (3.33) in return can be used to write the four modal parameters, see Equation (3.9), in terms of these four Dobson parameters as

$$\omega_r = \sqrt{\frac{-d_R u_R - d_I u_I}{u_R^2 + u_I^2}}, \tag{3.34}$$

$$\eta_r = \frac{d_R u_I - d_I u_R}{-d_R u_R - d_I u_I}, \tag{3.35}$$

$$A_r = \frac{u_R}{u_R^2 + u_I^2}, \tag{3.36}$$

$$B_r = -\frac{u_I}{u_R^2 + u_I^2}. \tag{3.37}$$

These might look familiar, as Equation (3.34) to (3.37) are almost equal to the modal parameter formulas from the line-fit method, Equation (3.17) to (3.20), where only A_r and B_r is multiplied with -1 (and other parameter names are used). This can be explained using the fact that the Dobson parameters, Equation (3.30) to (3.33), are equal to the line-fit parameters, see Appendix A.2 Equation (A.7) to (A.10), except for the fact that they are all multiplied with -1.

Equation (3.34) to (3.37) can be used to regenerate the measured FRF using Equation (3.9), as is done in the line-fit method in Chapter 3.4.2. This way, the correctness of the modal parameters can be checked, see also Figure 3.6.

3.5 Interference criteria

The proximity of other resonances can cause problems for the identification of the resonance of interest, as show the discussed identification methods. For MDOF systems with close eigenfrequencies, the interference magnitude criterion (IMC), as described in Chapter 3.2.1 "Interference criteria" of the PhD thesis of Maia [22], is a tool to see if two close modes interfere (substantially) with each other. For the IMC the half-power points of a resonance are of importance, which are defined at the receptance magnitude of $\frac{1}{\sqrt{2}}$ times the maximum receptance magnitude of the resonance, which are ω_{11}, ω_{21} and α_1 respectively in Figure 3.8.

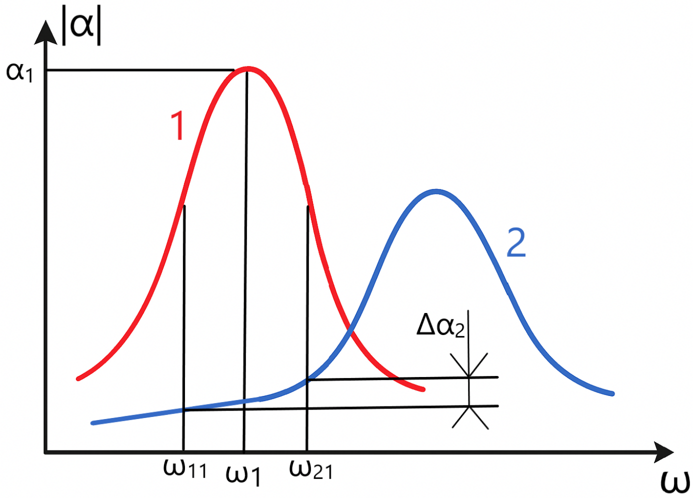

Figure 3.8: *Interference criteria definitions, in which ω_{11} and ω_{21} are the half-power points of mode 1*

The IMC deals with the different modes as if they were well-seperated and therefore Equation (3.9) is used to determine the rough modal properties of each resonance, after which the IMC tells how much these properties are affected by the other mode so how trustworthy they are in the end.
The interference magnitude criterion of a hysteretically damped system for the interference of mode 2 on mode 1 as in Figure 3.8 is

$$\frac{\Delta|\alpha_2|}{|\alpha_1|} \leq \nu_{abs} \tag{3.38}$$

$$\delta a^2 \left\{ \frac{1}{\sqrt{(\frac{1-a^2}{\eta_1} - a^2)^2 + \gamma^2}} - \frac{1}{\sqrt{(\frac{1-a^2}{\eta_1} + a^2)^2 + \gamma^2}} \right\} \leq \nu_{abs}, \tag{3.39}$$

in which $a = \frac{\omega_1}{\omega_2}$, $\gamma = \frac{\eta_2}{\eta_1}$ and $\delta = \frac{C_2}{C_1}$, see also Equation (3.10).
The dimensionless ν_{abs} defines the maximum value for the IMC for which the errors in the modal parameters found by identification of the resonance stay small. Maia [22] found that ν_{abs} could therefore have a value of at most 0.5%, so a maximum value of 0.005 for the IMC. As the Dobson's method was not yet published at this time, it is expected that this number only holds for the inverse-method and the line-fit method, because the Dobson's method is less sensitive to close modes.

From [22] it can be concluded that an increase in a, so mode 1 getting closer to mode 2, as well as an increase in δ, that is C_2 increasing relative to C_1, results in an increase in the IMC, thus giving more interference between the two modes.
Maia wrote "the influence of γ is very small", but based on the available data in his PhD thesis [22] this can possibly better be written as "the influence of changing just η_2 is very small", because no change of just η_1 was studied. Possibly, changing just η_1 was not needed, because the mathematics might show that just changing η_2 is enough to prove the influence of γ, but this was not studied during this master thesis. An increase in damping loss factor of the first mode, η_1, while keeping the damping ratio γ constant, will result in an increase in the IMC, Maia found. The damping loss factor η_r is related to the width of the resonance in the FRF, in which a higher damping will result in a wider resonance with a smaller height.

Besides the IMC, Maia [22] describes the interference phase criterion (IPC) to see if the phase of the receptance of different modes interfere with each other. Maia did not find a limit value for the ν_{phase} of this criterion and therefore it is not taken into account in this thesis. The IPC is described in Appendix A.4.

4 Modified Dobson's method

The Modified Dobson's method is developed by Di Maio [3] as a technique to capture the asymmetry of resonances in the receptance magnitude plot that can exist for non-linear eigenmodes. These are eigenmodes that do not show a linear relationship between the force on the system and the response that this gives. This makes the Modified Dobson's method differ from the Dobson's method, Chapter 3.4.3, that can only be used for linear modes.
First the Modified Dobson's method is described in Chapter 4.1. Secondly, the problems that arise with this method when a second close mode is present are discussed in Chapter 4.2. In Chapter 4.3 the effect on the Modified Dobson's method of making the distance between two modes smaller or larger is investigated.

4.1 Modified Dobson's method

The second line-fit that is done in the Dobson method in Chapter 3.4.3 uses many datapoints to establish a linear fit, as can be seen in the bottom row of Figure 4.1, where for simplicity of the figure only 13 datapoints are used. This could, however, also be done with just three datapoints in an iterative way. This technique forms the basis of the modified Dobson's method, compared to the "standard" Dobson's method.

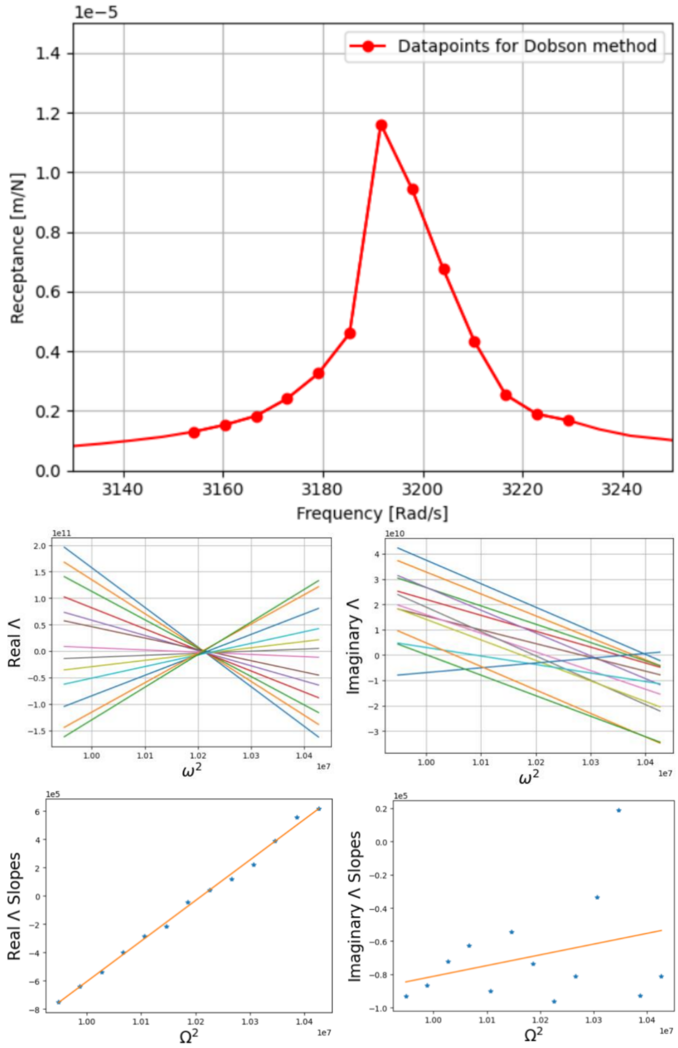

Figure 4.1: *Copy of Figure 3.7, example Dobson procedure: top row: datapoints from the measured receptance, middle row: Λ plotted as function of ω^2 with each line representing one Ω^2-value related to one of the datapoints above, bottom row: slopes of each Ω^2-line plotted as function of this Ω^2.*

Using only three datapoints means that there are also only three lines needed in the Re(Λ) and Im(Λ) plots respectively, see Figure 4.2, which shows an example of the middle row of Figure 4.1 for the Modified Dobson's method. The bottom row in Figure 4.1 then shows only three datapoints per figure, one for each Ω^2-line in the middle row. This results in a line-fit in the bottom row that is drawn through only three datapoints, which should in theory be located on one line according to Equation (3.28) and (3.29). The line-fit can then be used to calculate the Dobson parameters from Equation (3.30) to (3.33) like was done in the Dobson method.

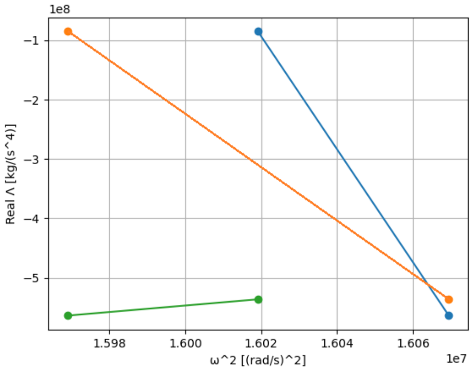

(a) *Three real Ω^2-lines coming from three datapoints*

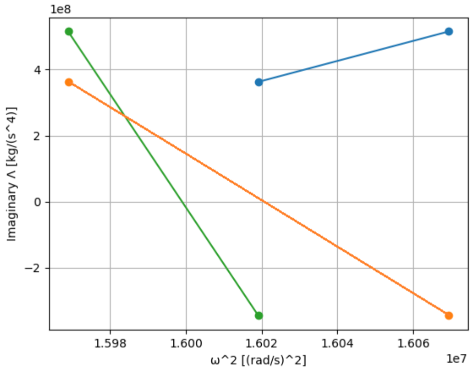

(b) *Three imaginary Ω^2-lines coming fron three datapoints*

Figure 4.2: *Example of the middle row in Figure 4.1 for a sweeper choice half way in between the fixer-locations in the Modified Dobson method, no datapoints in this graph for each $\Omega^2 = \omega^2$, as this Λ-value does not exist. The blue line is the Ω^2-line of Ω^2=1.597e7 $(rad/s)^2$, etc. The slope value of each of these lines is then plotted at its Ω^2 value in the bottom row of Figure 4.1.*

There are thus only three Ω^2 values needed for these lines, see Equation (3.23). The Ω^2 values should be close to the eigenfrequency squared ω_r^2 as discussed in Chapter 3.4.3. The three Ω^2 values that are used are the squares of three Ω values, each belonging to a certain datapoint. These are two so-called "fixers": datapoints with a relatively low receptance magnitude, one on either side of the resonance peak, and one datapoint that is called the "sweeper", for which its frequency is in between the frequencies of the fixers. In the top row of Figure 4.1 the fixers could be the first and the last datapoint that is being displayed, at roughly 3964 and 4040 rad/s respectively. The sweeper would then be one of the other datapoints, that is in between those two.

The Dobson parameters are then calculated for one sweeper with fixers combination. These parameters are subsequently used to calculate the four modal parameters using Equation (3.34) to (3.37). This way, the FRF can be regenerated for one sweeper-with-fixers combination.

It is, however, also possible to choose another sweeper in between the frequencies of the two fixers (which are not changed). For the top row of Figure 4.1 this would mean that there are 11 datapoints in between the two chosen fixers, which means that a total of 11 sweeper options exist. With another sweeper choice, the whole process starts over again and another FRF regeneration can be made in the end. For well-separated linear modes, these regenerations will be (almost) equal, but for non-linear modes this is not the case. This will be explained more extensively in Chapter 5.2, but it is related to the fact that a non-linear mode can have an asymmetric resonance, as can be seen for the white circles in Figure 4.3. The regenerations that are done using four modal parameters that are found each, result in symmetric resonances, even for analysing 3 datapoints of an asymmetric resonance. By repeating the process with a different sweeper choice every time, it is possible to capture this asymmetry, which is the goal of the Modified Dobson's method, by comparing the regenerations.

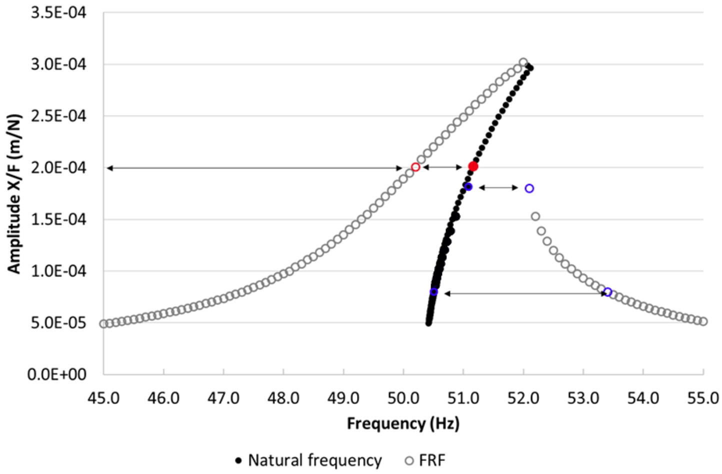

Figure 4.3: *Example of a backbone, plotted here in black dots, of an FRF of a nonlinear eigenmode, plotted as white circles, the magnitude receptance value of the sweeper is used as the y-coordinate for the natural frequency or eigenfrequency datapoint for the backbone, as shown in red and blue, 1 Hz = 2π rad/s, from [3], adjusted.*

For each sweeper choice, from the second to the second to last datapoint, there is thus a regeneration of a symmetric resonance possible using the four modal parameters that are calculated using this sweeper combined with the two fixers. The magnitude of receptance of datapoint can be formulated as

$$(|\alpha(\omega_0^{fxr})|, |\alpha(\omega_i^{swp})|, |\alpha(\omega_{N+1}^{fxr})|) \\ i = 1, ..., N, \tag{4.1}$$

in which fxr and swp stand for fixer and sweeper respectively, N is the number of datapoints in between the fixers, which is 11 in the example of Figure 4.1. ω_0 is the frequency of the preceding datapoint to the first sweeper datapoint, thus ω_0 is the frequency of the left fixer and ω_{N+1} is the frequency of the right fixer.
By writing $|\alpha(\omega_i^{swp})| = |\alpha_i^{swp}|$ this results in

$$\omega_r(|\alpha_i^{swp}|)\,, \tag{4.2}$$

$$\eta_r(|\alpha_i^{swp}|)\,, \tag{4.3}$$

$$A_r(|\alpha_i^{swp}|)\,, \tag{4.4}$$

$$B_r(|\alpha_i^{swp}|)\,, \tag{4.5}$$

such that each of the four modal parameters becomes a function of the sweeper receptance magnitude (which depends in the end on the sweeper frequency) [3]. These functions can be investigated each on their own.

In case of an isolated linear mode in a MDOF FRF, which can be treated as an SDOF FRF, see Chapter 3.3, the effect of the sweeper receptance/frequency on the modal parameters is neglectible. In case of a perfect system with perfect measurements, the effect is non-existent, so each sweeper receptance/frequency will result in the exact same modal parameters and Equation (4.2) to (4.5) are thus all constants. When there is a little error in the measurements and/or the system is not perfect, some variations in the modal parameters will be seen for different $|\alpha^{swp}|$ values.

In case of an isolated nonlinear asymmetric mode like the white circles in Figure

4.3 from [3] in an MDOF FRF, which can be treated like an SDOF FRF, there is a clear effect of the sweeper receptance/frequency. For instance, the eigenfrequency $\omega_r(|\alpha^{swp}|)$ that is found shows a clear dependency on the sweeper that is chosen. This is best shown by taking the receptance magnitude value $|\alpha^{swp}|$ of the specific sweeper point and plotting this as a function of the eigenfrequency ω_r that is found using this sweeper. This will generate a graph that is called the backbone of the mode, see the black dots in Figure 4.3, where the backbone is plotted in the same graph as the FRF measurement. Here it will show, in the ideal measurement situation, the curved line that lays around average in the curved asymmetric nonlinear eigenmode shape, as is seen in Figure 4.3. This makes the backbone a good means of showing such asymmetries.
The backbone can also be plotted for linear modes, which is the focus of this report up till here, for non-linear modes, see Chapter 5.2. The backbone for an isolated linear mode shows a vertical line, as the mode is linear, so there is no asymmetry in its resonance in the FRF.

4.2 Problem description

The Modified Dobson's method works satisfactorily when the eigenfrequencies are far apart from each other [3], but for closer modes, it fails. As will be discussed in Chapter 5.2, this was seen for nonlinear modes, for which the Modified Dobson's method was designed, with a close second mode. Failing of the Modified Dobson's method was also seen for linear modes that are close to eachother, which will be focused on here for simplicity.

For well-separated linear modes, the regenerations with the Modified Dobson method using the results of each of the sweeper positions will be (almost) equal, as described in Chapter 4.1. However, with a second mode closer to the mode that is investigated, these regenerations will not be equal, which is caused by the residual from other modes that is assumed to be constant, but it is not, as can be seen for example in Figure 3.3 in Chapter 3.3. Like the Dobson's method, the Modified Dobson's method assumes the residual R in Equation (3.14) and (3.21) to be constant around the eigenfrequency of interest, this makes this method sensitive to close other modes, for which this residual cannot be assumed constant.

The problem with close modes can also be visualised with a simple artificial FRF of linear modes, to make it more clear. Here the first mode has the modal constants A_1=2 kg^{-1} and B_1=4 kg^{-1} and a damping value of η_1=0.002. The eigenfrequency of the first mode is located at 3000 rad/s, so ω_1=3000 rad/s. The second mode has the same modal constants and damping value of A_2=2 kg^{-1}, B_2=4 kg^{-1} and η_2=0.002 respectively. Its eigenfrequency, however, is varied to see the effect of the distance between the 2 modes, starting with an eigenfrequency of ω_2=4000 rad/s, so 33.33% higher than the first eigenfrequency. In Figure 4.4 the two resonances are plotted, they can be summed due to the principle of linear superposition, which holds in the basis for linear modes [1].This means that the responses of one resonance, for instance at 3500 rad/s, could be added to the response of the other resonance at this frequency, which will result in the total response. As the modal constants A_r and B_r of both resonances are equal, these vectors can point in opposite directions in the Nyquist plot when the resonances are in anti-phase. This is what is happening at 3500 rad/s in Figure 4.4 and causes the anti-resonance that is seen here. The maximum receptance magnitude of the second resonance is lower than that of the first, which could also be verified (analytically), see Appendix A.3. This might seem undesirable, but it allows to keep the modal parameters, except for the eigenfrequency, constant, while varying the eigenfrequency of the second resonance. In this way, a fair comparison of the frequency distances between the resonances can be made, also in the context of the IMC of Chapter 3.5.

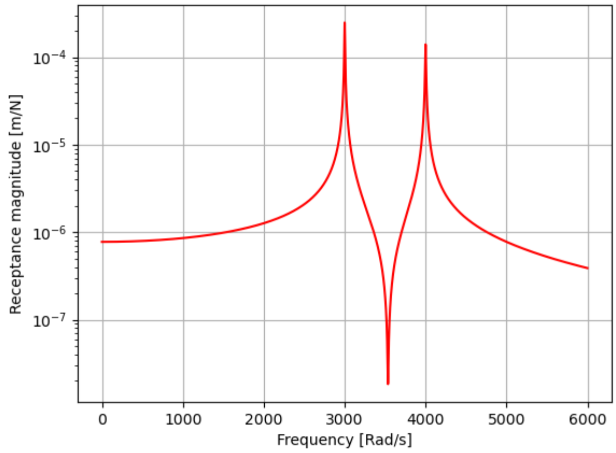

Figure 4.4: *Two resonances of linear modes that are too close to each other for a perfectly executable Modified Dobson's method.*

The fixer locations are chosen at a low receptance magnitude on the first resonance peak of linear mode, as this is how the Modified Dobson's method operates. Referring back to the skewed resonance of Figure 4.3, the fixers are located at the part of the resonance curve that would look similar in case the mode would have been linear [3]. This region is at a low receptance magnitude, think of below 5E-05 in Figure 4.3. The location of the fixers for the first resonance, from the two linear modes in Figure 4.4, that is analysed can be seen in Figure 4.5.

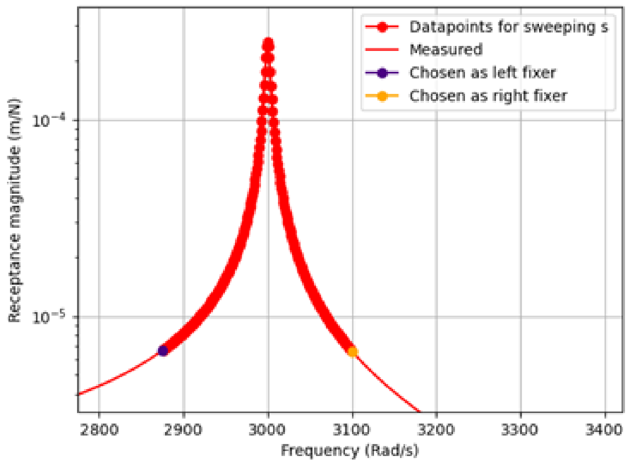

Figure 4.5: *Fixer locations for analysing the first resonance of a linear mode in Figure 4.4, "s" stand for sweeper-point here and "Measured" means datapoints that are not used in the analysis and are therefore plotted as a line.*

For the Modified Dobson's analysis of the first resonance of Figure 4.4 with the fixers locations of Figure 4.5 the regenerations resulting from each sweeper position are not equal. In Figure 4.6 it can clearly be seen that the backbone, $|\alpha^{swp}|$ over $\omega_r(|\alpha^{swp}|)$, splits into two tails at the bottom. The regeneration using the input of the first and last sweeper resulted in the lowest and highest eigenfrequency, respectively. A very similar phenomenon was also seen for non-linear modes, which will be discussed in more detail in Chapter 5.2. As a check, the same analysis was done for an FRF which consists of only the first eigenfrequency at 3000 rad/s from Figure 4.4. This resulted in the purple graph in Figure 4.6, which does show that all regenerations using the Modified Dobson's method for an SDOF linear system have equal eigenfrequencies. Although the splitting of the backbone of the first resonance of the MDOF linear system with the second resonance 1000 rad/s apart from the first, in red in Figure 4.6, is relatively minor, smaller than one per mille of the eigenfrequency, the effect increases with a smaller distance between the two resonances in Figure 4.4.

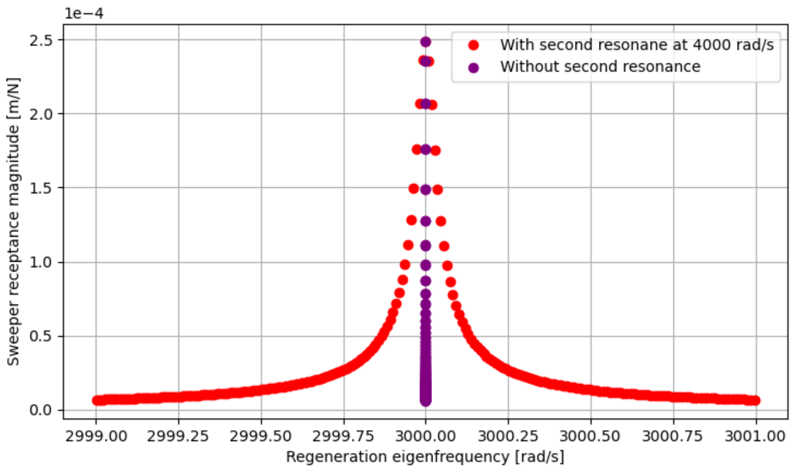

Figure 4.6: *Backbone splitting up with a second mode getting "close" to the mode at 3000 rad/s that is investigated*

4.3 Effect of the distance between two eigenfrequencies

The effects of a non-constant residual of another mode on the Modified Dobson's method are studied mathematically in Appendix A.5, but this mathematics is rather complicated and no clear image of the effects is found in here. Therefore, a more empirical approach is chosen to use instead of an analytical approach.

4.3.1 Regeneration eigenfrequency

To show that the severity of the backbone splitting increases with a smaller distance between two eigenfrequencies, several simulations were done, each with a different frequency distance.
To make a fair comparison between the different eigenfrequency distance cases, the fixer locations were taken at the same height relative to the resonance peak height each time. A commonly used measure for taking a certain bandwidth of a resonance are the half-power points, which are located at the level of the maximum receptance magnitude $|\alpha_r|_{\max}$ divided by $\sqrt{2}$ [1, 4] and are also used in the IMC in Chapter 3.5. The half-power points were too high up the resonance peak, as they would be even above the 10^{-4} m/N receptance magnitude line in Figure 4.5, which is clearly not close to the height of the fixers in that picture. A different measure therefore had to be come up with, that would be located in a lower region that would count as the linear region in case of a skewed resonance of nonlinear mode like in Figure 4.3. This measure became the one-thousandth power points, defined as the points on the resonance at a level of the maximum receptance magnitude $|\alpha_r|_{\max}$ divided by $\sqrt{1000}$. The definition of the maximum receptance magnitude $|\alpha_r|_{\max}$ can be seen in

Appendix A.3.

The fixer locations in Figure 4.5, that was used to visualise the problem of close modes, are close to the one-thousandth power points. For the remainder of this report, the fixers are taken at the one-thousandth power points, including for the case of second resonance at a eigenfrequency of 4000 rad/s, so 33.33% higher than the first eigenfrequency. This allows for a fair comparison between the different eigenfrequency distances. The distance between the resonances was halved several times, that is 1000, 500, 250 and 125 rad/s, to see the effect of this on the Modified Dobson's analysis. An example of the fixer locations is given in Figure 4.7.

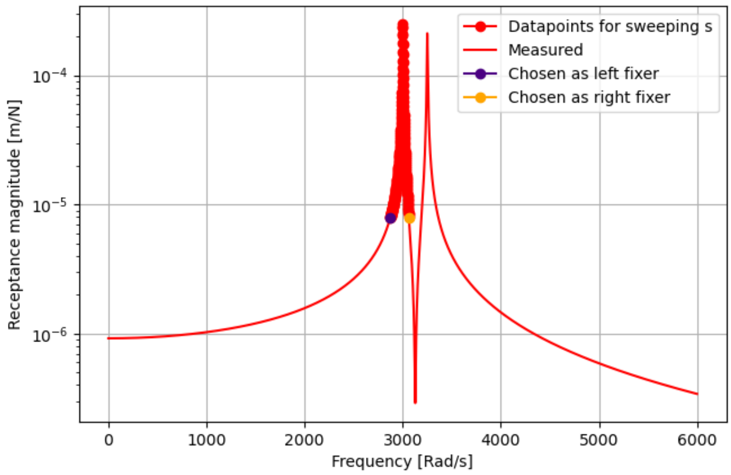

Figure 4.7: *Fixer locations at the one-thousandth points for 250 rad/s distance between the resonances, "s" stand for sweeper-point here and "Measured" means datapoints that are not used in the analysis and are therefore plotted as a line*

The backbone of the first resonance for each of the cases of a second resonance at a relative distance to the eigenfrequency of the first resonance is plotted in Figure 4.8. It visualises the spread of the regeneration eigenfrequencies, which is increasing for a closer second resonance.

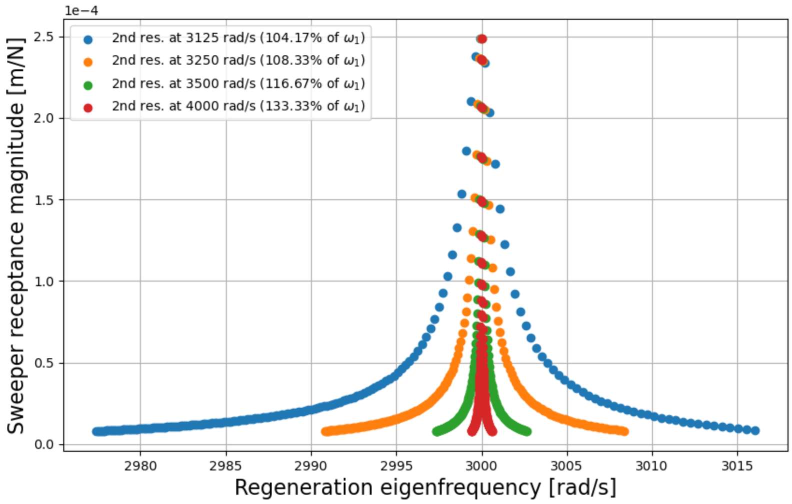

Figure 4.8: *Backbone splitting up for the cases of a second mode at 125, 250, 500 and 1000 rad/s distance from the 3000 rad/s mode investigated*

The average regeneration eigenfrequency results of the Modified Dobson method for the different distances between the resonances are given in Figure 4.9. In here, the eigenfrequency of the second resonance is plotted on the x-axis as a percentage of the eigenfrequency of the first resonance. Figure 4.9 shows that the average regeneration eigenfrequency is getting increasingly off from the theoretical for a decreasing distance between the resonances, although the absolute error is small and does not exceed 0.30% for these simulations.

A similar plot as Figure 4.9 is made for the standard deviation σ of the regeneration eigenfrequency ω_1 in Figure 4.10. The standard deviation increases with a decreasing distance between the resonances. This means that the width of the backbone split is increasing, as the x-values of the backbone are the regeneration eigenfrequencies, which can also be seen in Figure 4.8. Although an increase in standard deviation is seen, the absolute spread is small and the standard deviation does not exceed 0.40% of the theoretical eigenfrequency ω_1 for these simulations.

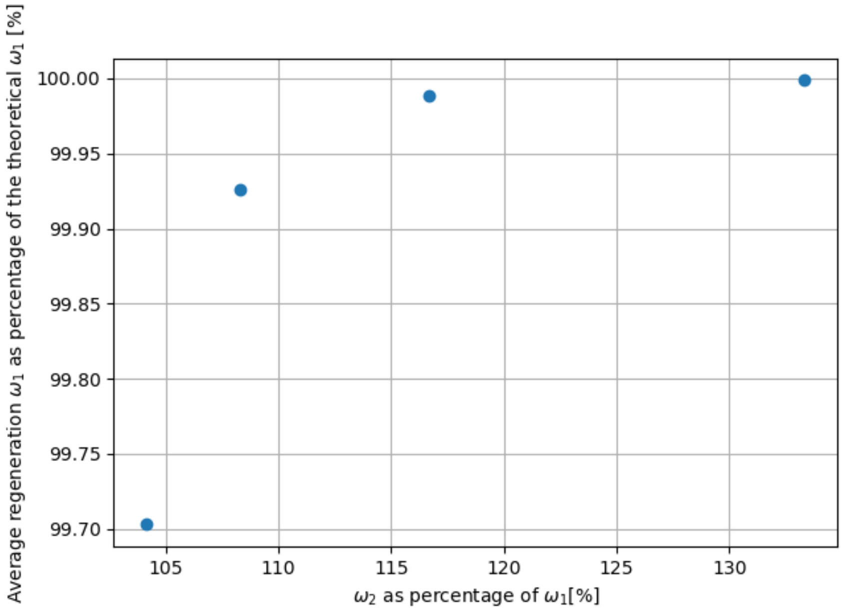

Figure 4.9: *Analysis of the data of Figure 4.8: Average regeneration eigenfrequency ω_1 as percentage of the theoretical ω_1 as a function of the eigenfrequency ω_2 of the second resonance as percentage of ω_1 of the first resonance*

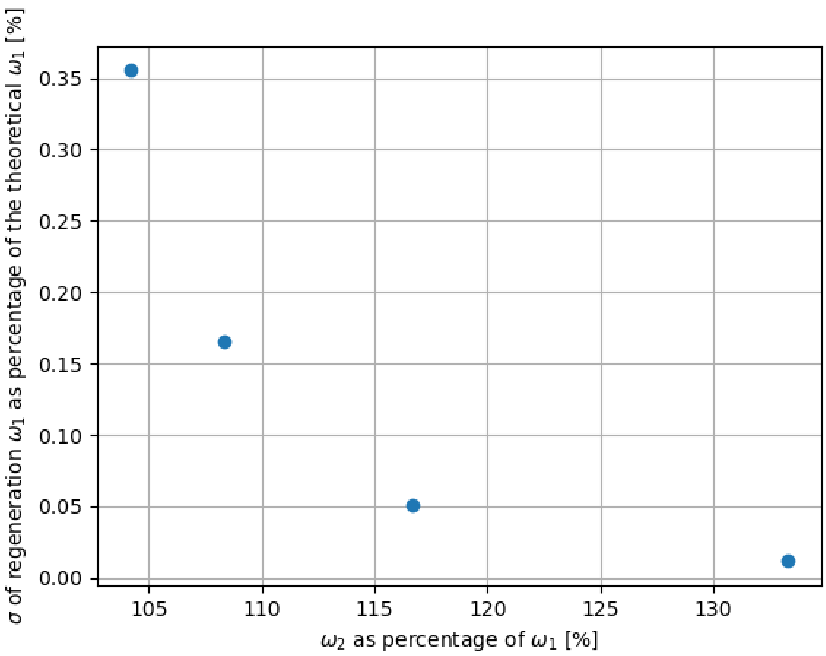

Figure 4.10: *Analysis of the data of Figure 4.8: Standard deviation σ of the regeneration eigenfrequency ω_1 as percentage of the theoretical ω_1 as a function of the eigenfrequency ω_2 of the second resonance as percentage of ω_1 of the first resonance*

4.3.2 Other modal parameters

Besides the eigenfrequency, also other modal parameters are calculated with the Modified Dobson's method for each regeneration, see Equation (4.2) to (4.5), which are the damping loss factor η_r and the modal constants A_r and B_r. The magnitude receptance of the sweepers ,$|\alpha^{swp}|$, can be plotted as a function of these modal parameters, as was done for the regeneration eigenfrequencies that formed the backbones in Figure 4.8.

The regeneration damping loss factor η_1 results for different distances between the resonances are given in Figures 4.11 and 4.12. Figure 4.11 shows that the average regeneration damping loss factor is rather close to the theoretical 0.002 value for the second resonance at 4000 rad/s (133.33% of ω_1) case. It becomes less close however, for resonances that are closer to the first resonance. For the case of a second resonance at 3125 rad/s (104.17% of ω_1), η_1 becomes even higher than the 0.002 value, although a trend for a decreasing value can be seen for the others. The fact that the average for the 125 rad/s distance is higher is caused by a large tail with many datapoints, like in Figure 4.8, that pull the average upwards. Figure 4.12 show that the standard deviation σ of the regenerated η_1 increases for a smaller distance between the resonances, indicating that the tails of the graph are increasing in width, which can also be seen in Figure 4.13.

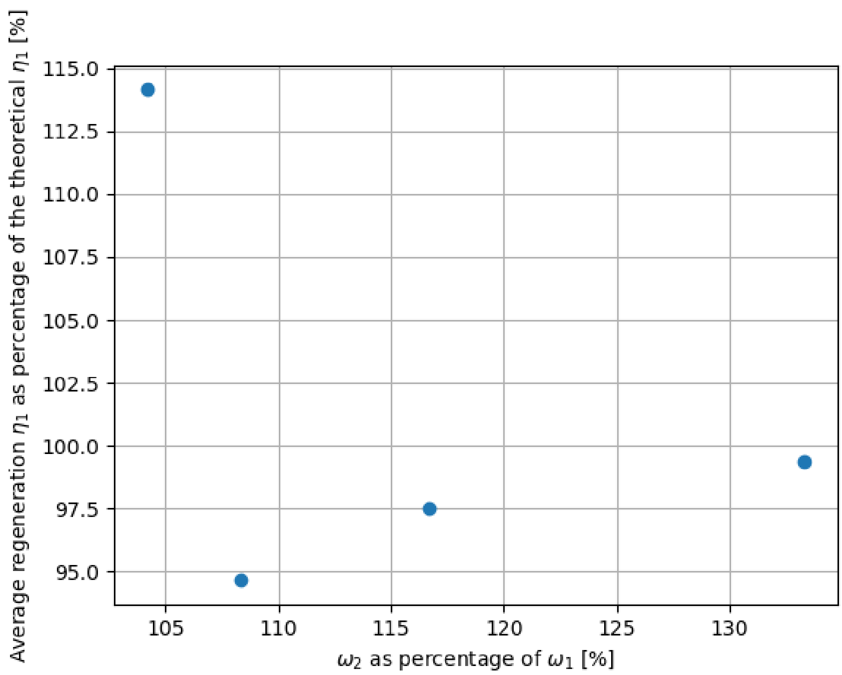

Figure 4.11: *Analysis of the results of the Modified Dobson's method: Average regeneration damping loss factor η_1 as percentage of the theoretical η_1 as a function of the eigenfrequency ω_2 of the second resonance as percentage of ω_1 of the first resonance*

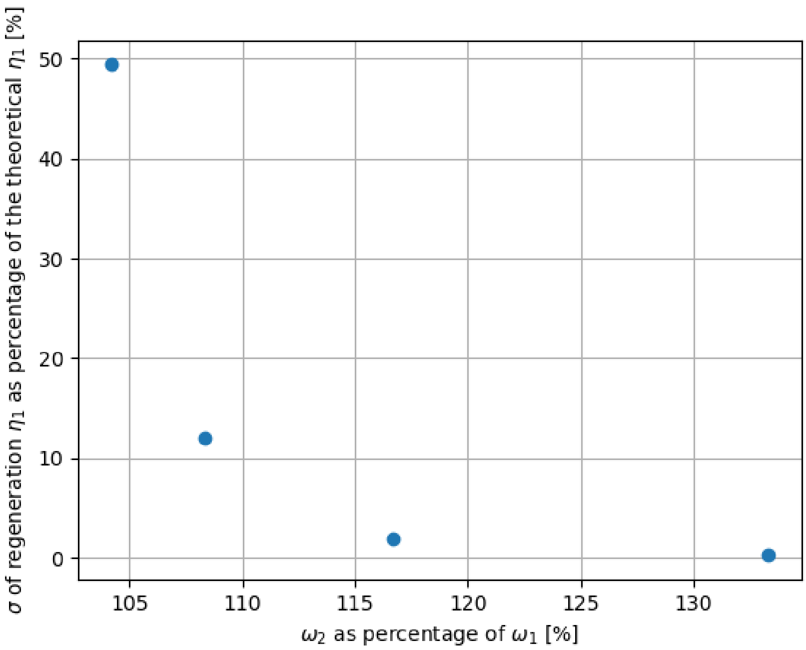

Figure 4.12: *Analysis of the results of the Modified Dobson's method: Standard deviation σ of the regeneration damping loss factor η_1 as percentage of the theoretical η_1 as a function of the eigenfrequency ω_2 of the second resonance as percentage of ω_1 of the first resonance*

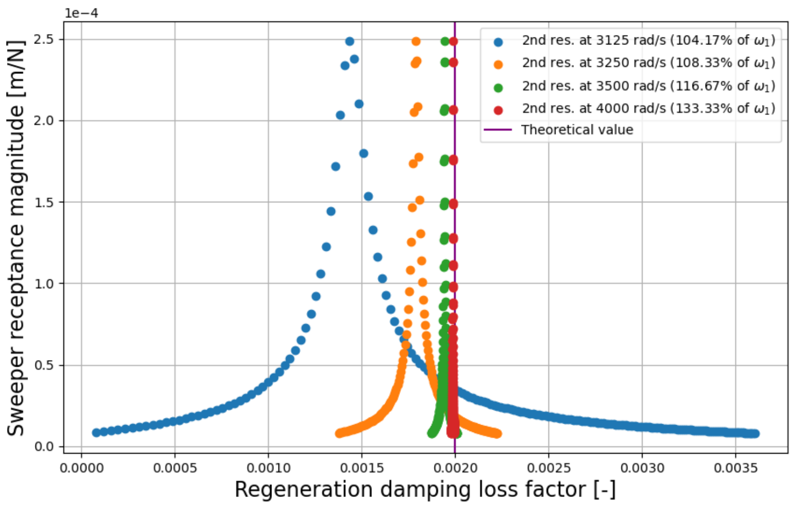

Figure 4.13: *Sweeper receptance magnitude as function of the regeneration damping loss factor η_1 of the first resonance at 3000 rad/s for the cases of a second resonance at 125, 250, 500 and 1000 rad/s distance, the theoretical damping loss factor has a value of 0.002 and is depicted by the vertical purple line.*

The regeneration modal constants A_1 and B_2 results for different distances between the resonances are given in Figures 4.14 and 4.15. In Figure 4.14, the average regeneration modal constants A_1 and B_1 for the second resonance at 4000 rad/s (133.33% of ω_1) case are rather close to the theoretical 2 kg^{-1} and 4 kg^{-1} respectively. This again becomes less close for a decreasing distance between the resonances, where a clear decrease in the average regeneration values of both A_1 and B_1 can be seen, but this decrease is stronger for A_1. The standard deviations of the results increase roughly similarly for A_1 and B_1 for a smaller distance between the resonances, as can be seen in Figure 4.15, which is caused by the tails of the graph increasing in width. This increase in de width of the tails can also be seen in Figure 4.16 and 4.17.

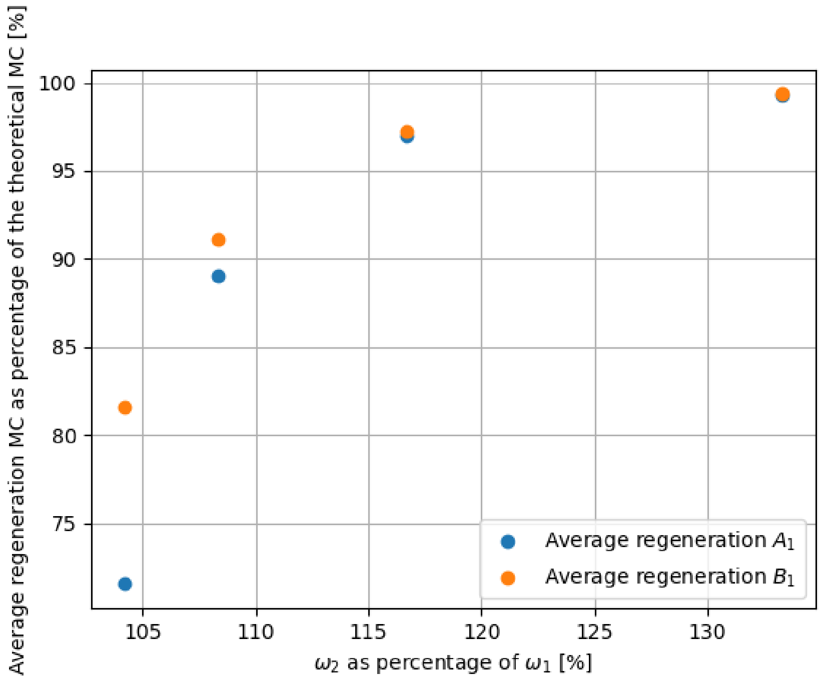

Figure 4.14: *Analysis of the results of the Modified Dobson's method: Average regeneration modal constants (MC) A_1 and B_1 as percentage of the theoretical MC A_1 and B_1 respectively, as a function of the eigenfrequency ω_2 of the second resonance as percentage of ω_1 of the first resonance*

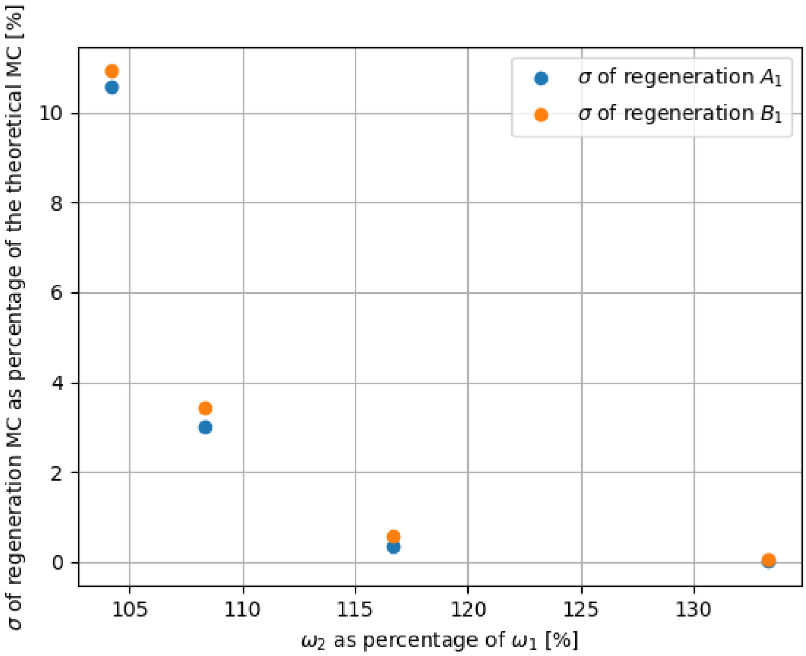

Figure 4.15: *Analysis of the results of the Modified Dobson's method: Standard deviation of the regeneration modal constants (MC) A_1 and B_1 as percentage of the theoretical MC $A1$ and B_1 respectively, as a function of the eigenfrequency ω_2 of the second resonance as percentage of ω_1 of the first resonance*

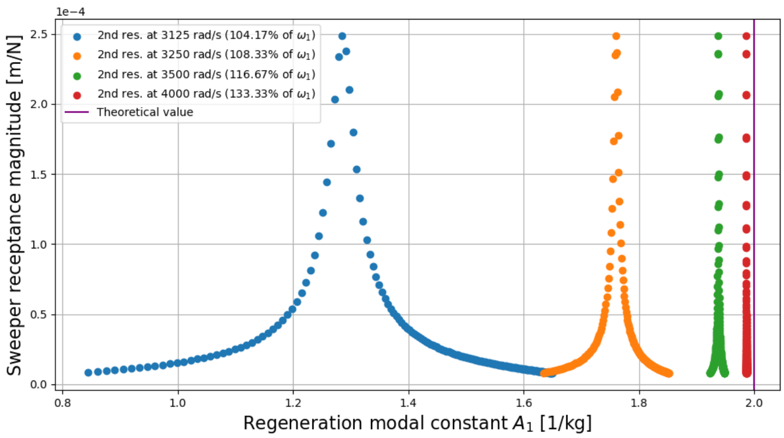

Figure 4.16: *Sweeper receptance magnitude as function of the regeneration modal constant A_1 of the first resonance at 3000 rad/s for the cases of a second resonance at 125, 250, 500 and 1000 rad/s distance, the theoretical modal constant A_1 has a value of 2 kg^{-1} and is depicted by the vertical purple line.*

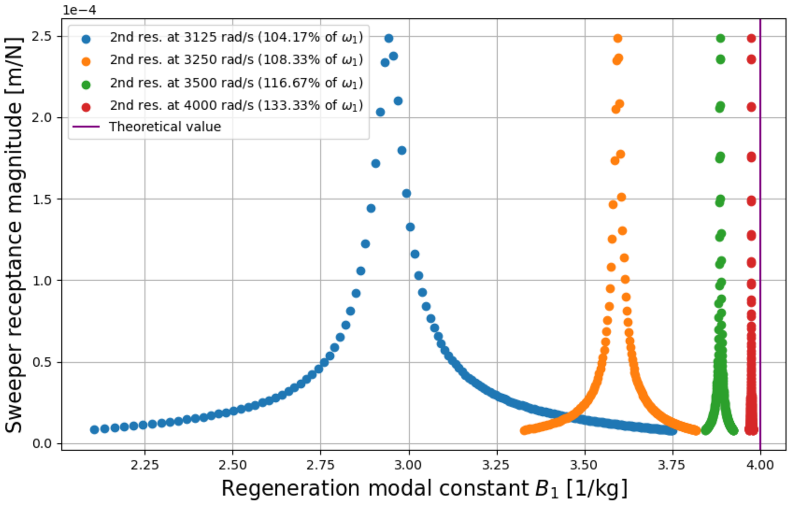

Figure 4.17: *Sweeper receptance magnitude as function of the regeneration modal constant B_1 of the first resonance at 3000 rad/s for the cases of a second resonance at 125, 250, 500 and 1000 rad/s distance, the theoretical modal constant B_1 has a value of 4 kg^{-1} and is depicted by the vertical purple line.*

4.3.3 Interference magnitude criterion

When looking back at the IMC in Chapter 3.5 this could also be computed for the close modes in this chapter using Equation (3.39). The results can be seen in Figure 4.18. The IMC values are all clearly below the maximum of 0.005 that Maia [22] found for the line-fit method. There is thus no problematic magnitude interference seen for these resonance distances for the line-fit method. For the Modified Dobson's method however, there are clear interference problems as shown in this chapter. Only for the second resonance at 4000 rad/s (133.33% of the ω_1), all four averages of the modal parameters are within 1% margin of the theoretical values and the magnitude interference could therefore be classified as minor. This means that the maximum value of the IMC for the Modified Dobson's method needs to be much lower than for the line-fit method. Based on the result in Figure 4.18, the IMC could be somewhere between 0.0000132 (133.33% case) and 0.0000613 (116.67% case) instead of the 0.005 for the line-fit method. More research would be needed however, to determine this number more trustworthy, in which the also the more simulations could be taken into account, also with different damping values for instance. According to the theory from Chapter 3.5 the IMC increases for a higher damping of both resonances while keeping the ratio between the two constant, so more distance between the resonances is needed in that case.

For the calculation of the IMC, the exact modal parameters were used, as they were known. For experimental FRF data, this is not the case and approximations of the modal parameters of each resonance have to be used. This will decrease the precision of the calculated criterion, which is something to take into account.

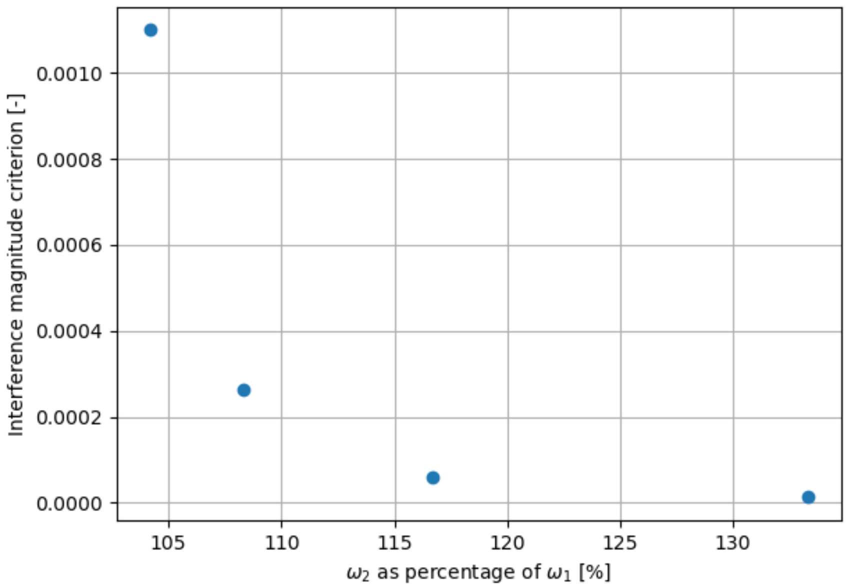

Figure 4.18: *Analysis of the results of the Modified Dobson's method: Interference magnitude criterion [-] as a function of the eigenfrequency ω_2 of the second resonance as percentage of ω_1 of the first resonance*

4.4 Conclusion

It can be concluded that the modal parameters, including the list of eigenfrequencies ω_1, that are found with the Modified Dobson's method become increasingly less accurate for a decrease in the distance between resonances of linear systems. This means that, for example, the regeneration damping graph is shifted towards a damping value that is not the damping loss factor of the resonance. Besides this, also the spread of the regenerated modal parameters increases, which makes that for instance the backbone starts splitting, decreasing the clarity of a possible backbone of a skewed resonance in case of a nonlinear system. The backbone in Figure 4.3 becomes less distinct in that case. The maximum IMC value to see minimal interference between the resonances turns out to be much lower for the Modified Dobson's method compared to the line-fit method that the IMC was designed for by Maia [22]. Besides the distance between the resonances, also the damping of the resonances is of influence on the IMC. According to the theory of the IMC, it increases for a higher damping of both resonances while keeping the ratio between the two constant, so more distance between the resonances is needed in that case to stay below the maximum IMC value.

5 Proposal to reduce the residual from other modes

This chapter describes the proposal that was created during this project to reduce the residual coming from other modes. It is expected that this will result in cleaner results for the Modified Dobson's method. The proposed solution is described in Chapter 5.1. Chapter 5.1.1 describes the best sweeper to pick for the regeneration that is needed for this solution. Subsequently, this regeneration is subtracted from the total receptance in Chapter 5.1.2. Then the Modified Dobson's method is used on the result of this subtraction in Chapter 5.1.3, where the results are also compared to those of Chapter 4. Chapter 5.2 describes the analysis of nonlinear resonances, in which a link is made with the proposed solution. At the end a conclusion is given in Chapter 5.3.

5.1 Proposed solution

A solution was proposed to decrease the sensitivity of close other modes for the Modified Dobson's method. For this idea, Equation (3.8) is shown again, the total FRF response of multiple linear modes is

$$\text{total-FRF} = \sum_{r=1}^{N} \alpha_r(\omega) = \sum_{r=1}^{N} \frac{A_r + iB_r}{\omega_r^2 - \omega^2 + i\eta_r\omega_r^2}. \tag{5.1}$$

The proposed solution is: regenerate a mode close to the mode of interest as good as possible, for which a proposed procedure will be given, use this regeneration to approximate the residual coming from this close mode and subtract this residual from the total receptance in the region of the mode of interest . This is possible, as Equation (5.1) shows that the FRF that is being measured is a sum of all the eigenmodes. Subtracting all the other modes from the FRF will therefore, theoretically, give the exact eigenmode that is of interest. The "cleaner" resonance, after the subtraction of the estimation of the residual of the other mode(s), will have more similarities with an isolated linear mode than before subtraction. The receptance model of a single resonance in an MDOF linear system is:

$$\alpha(\omega) = \frac{A_r + iB_r}{\omega_r^2 - \omega^2 + i\eta_r\omega_r^2} + R(\omega), \tag{5.2}$$

where R is the residual receptance coming from other modes, as was also shown in Equation (3.14). This residual is assumed to be constant for the Modified Dobson's method. As this method only works properly for an isolated mode, moving to a more isolated situation in which the residual from other modes approaches a constant, is expected to improve the results. This makes that it is expected that using the Modifed Dobson's method, the backbone, among others, will show less severe splitting compared to not doing any subtraction.

It was decided to use one of the many regenerations of the Modified Dobson method to regenerate a second mode, which is linear. This can result in a less accurate regeneration than with, for instance, the Dobson method, but it has some advantages within this research. Although the analysis of the second mode with the Modified Dobson's method will be affected by the first mode, just like is the case the other way around, it is easier for the programming in Python to do all analyses with the same method. Besides this, investigating which of the many regenerations from a single Modified Dobson's analysis is most accurate will result in valuable insights in the Modified Dobson's method procedure, like which regeneration is most accurate.

5.1.1 Sweeper selection for the best regeneration

Where the classical Dobson method, Chapter 3.4.3, gives four modal parameters when analysing a certain mode, the Modified Dobson method in Chapter 4 gives these four modal parameters for each sweeper-fixer combination. This makes that there is not one single regeneration of the result, using these four modal parameters, but a possible regeneration for each sweeper.
To subtract a linear mode from the total FRF as well as possible, the best regeneration of this mode needs to be chosen from all these regenerations. This means that the sweeper out of all sweepers that gives the best regeneration needs to be found. The second resonance from the case of a second resonance at 3125 rad/s (104.17% of ω_1) from Chapter 4 was chosen to search for this best regeneration. The fixers for this Modified Dobson's analysis were again taken at the one-thousandth power points. The top of this resonance can be seen in Figure 5.1.

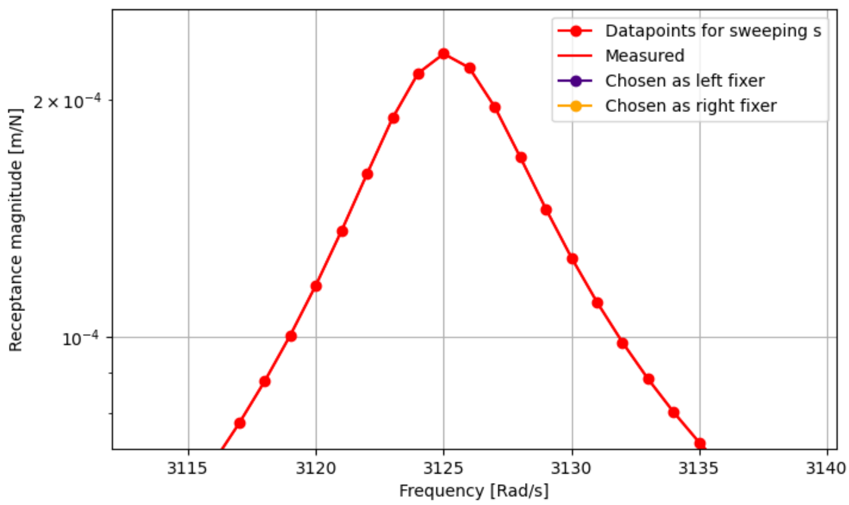

Figure 5.1: *Sweeper points "s" for the second resonance from the case of a second resonance at 3125 rad/s (104.17% of ω_1) from Chapter 4, the fixers at the one-thousandth power points are not shown in this zoom.*

In Figure 5.2 to 5.5 the results for the Modified Dobson's analysis on the example of Figure 5.1 for the second resonance at 3125 rad/s are given.
The plots show the sweeper receptance magnitude as a function of a regenerated modal parameter, for instance, the regenerated eigenfrequency ω_2 for the backbone plot in Figure 5.2. The red and purple dots in the plots show the results coming from the first and last sweeper respectively. The yellow dots show the results coming from the middle sweeper out of the list of sweepers. This corresponds to the middle frequency between the fixers, as the sweepers are spread evenly over the frequency, see also Figure 5.1. Looking at Figure 5.2, it can be seen that the sweeper with the highest receptance magnitude, which would be the sweeper at 3125 rad/s in Figure 5.1, resulted in the most accurate regeneration eigenfrequency ω_2. This could have been expected, as this sweeper is on the theoretical eigenfrequency and it has the highest receptance magnitude, so it clearly shows where the eigenfrequency is located. In

Figure 5.3, this highest magnitude sweeper does not result in the most accurate regeneration damping loss factor η_2 and the middle sweeper result is even a bit closer to the theoretical value. The regeneration modal constant A_2 for the last sweeper is more accurate than for the middle sweeper result and much more accurate than the result of the sweeper with the highest receptance magnitude, see Figure 5.4. Figure 5.5 shows that theoretical value of the regeneration modal constant B_2 is not in the range of the sweeper results, however, the result of the last sweeper would be the closest.

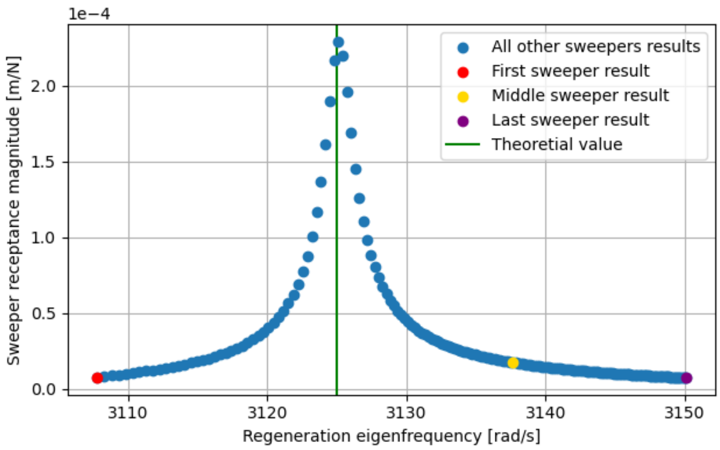

Figure 5.2: *Backbone of the second resonance for the case of a second resonance at 125 rad/s distance from the other resonance, the theoretical eigenfrequency is 3125 rad/s and is depicted by the vertical green line.*

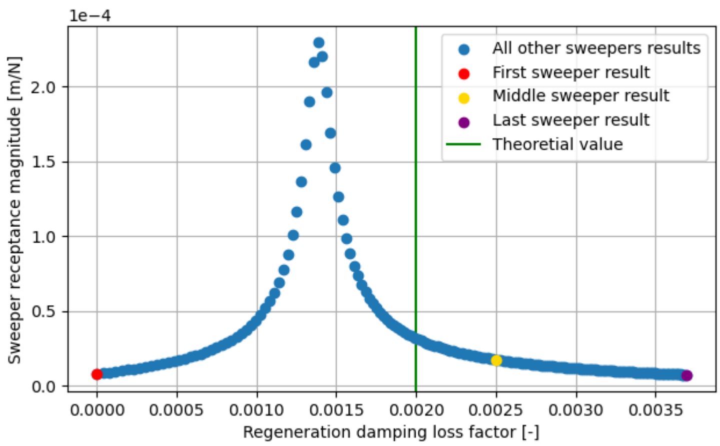

Figure 5.3: *Sweeper receptance magnitude as function of the regenerated damping loss factor η_2 of the second resonance for the case of a second resonance at 125 rad/s distance from the other resonance, the theoretical damping loss factor has a value of 0.002 and is depicted by the vertical green line.*

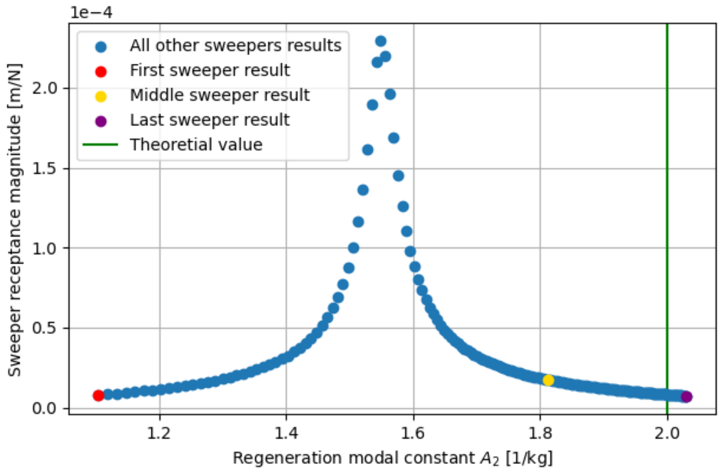

Figure 5.4: *Sweeper receptance magnitude as function of the regenerated modal constant A_2 of the second resonance for the case of a second resonance at 125 rad/s distance from the other resonance, the theoretical modal constant A_2 has a value of 2 kg^{-1} and is depicted by the vertical green line.*

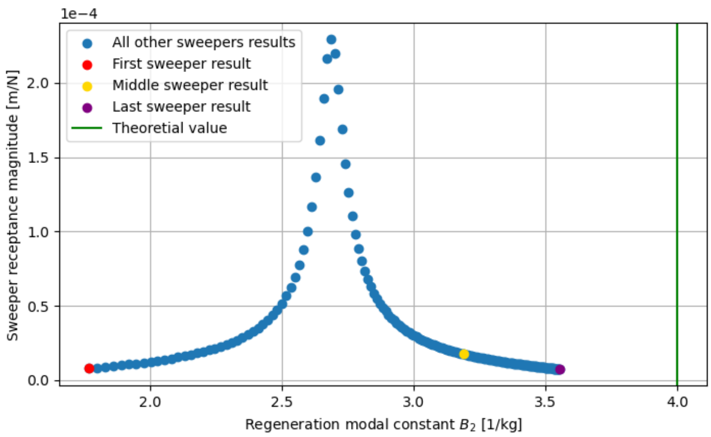

Figure 5.5: *Sweeper receptance magnitude as function of the regenerated modal constant B_2 of the second resonance for the case of a second resonance at 125 rad/s distance from the other resonance, the theoretical modal constant B_2 has a value of 4 kg^{-1} and is depicted by the vertical green line.*

A trade-off between the accuracy of the different modal parameters thus has to be found here. The equation of an MDOF linear system that could be approximated with an SDOF system is

$$\alpha(\omega) = \frac{A_r + iB_r}{\omega_r^2 - \omega^2 + i\eta_r\omega_r^2}, \tag{5.3}$$

as was also shown in Equation (3.9). It can be seen that $\alpha \propto 1/\omega_r^2$, which means that ω_r has a larger influence on the receptance than each of the other modal parameters, A_r, B_r and η_r, on their own. This was also seen when looking just at the maximum resonance magnitude, as was done in Appendix A.3. The regeneration eigenfrequency ω_r is thus an important parameter to focus on for regenerating the resonance as precisely as possible. Therefore it was chosen to use the sweeper with the highest receptance magnitude, which gives the most precise regeneration eigenfrequency as can be seen in Figure 5.2. This highest receptance magnitude did not give the most precise results for the other modal parameter plots in Figures 5.3 to 5.5, but they are also not the worst sweeper points to pick. Again, some trade-off had to be found.

The reason that this highest magnitude sweeper seemed to give the best result could be that this sweeper is relatively less affected by residuals of other modes, because of its relatively high receptance magnitude. For a sweeper closer to one of the two fixers, so at a lower receptance magnitude level, the effect of this residual is relatively larger.

As this sweeper choice seemed to give the best regeneration, it is expected that this regeneration will also approximate the residuals coming from this resonance that affect other modes the best as possible. The regenerated second resonance, for the 125 rad/s distance case from Chapter 4, using the highest magnitude sweeper, can be seen in Figure 5.6. A zoom-in at the top of the second resonance curve can be seen in Figure 5.7, which uses a similar scale as Figure 5.1. Here it can be seen that especially for the sweeper points around the top (all one rad/s apart from each other) the regenerated is very precise. Further away from the top the regeneration is less accurate and the difference in magnitude increases.
By subtracting the regenerated second resonance, the Modified Dobson's method could give more precise and more consistent results for the first resonance, as that one is less affected by the residuals from the second mode.

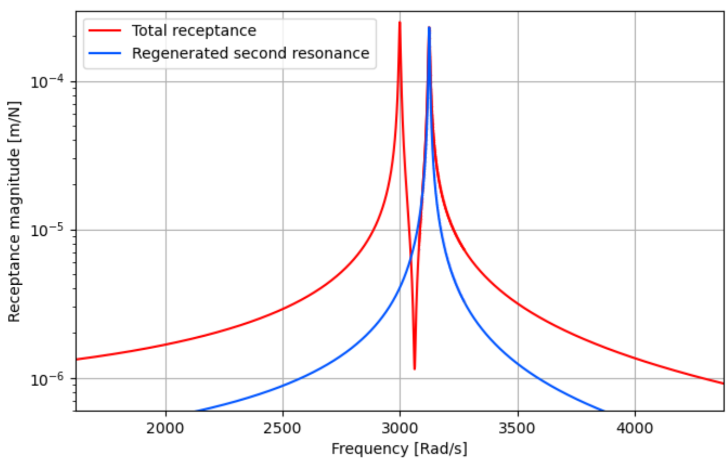

Figure 5.6: *Regenerated second resonance using the modal parameters from the highest magnitude sweeper for one-thousandth power points as fixers on the second resonance. Original receptance with two resonances plotted as well.*

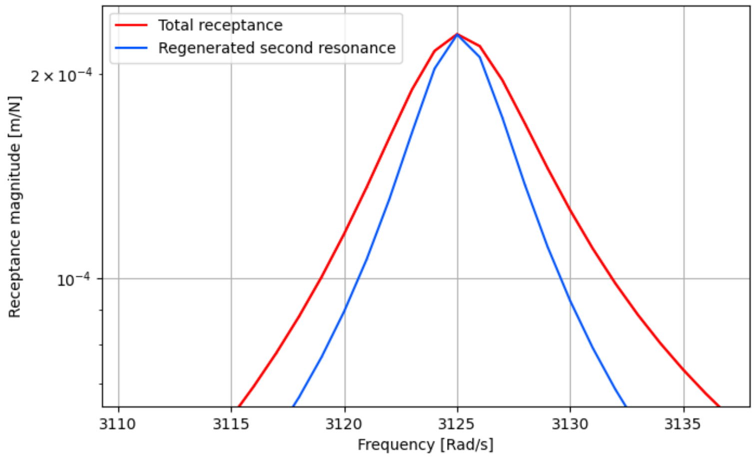

Figure 5.7: *Zoom-in at the top of the regenerated second resonance of Figure 5.6 that was made using the modal parameters from the highest magnitude sweeper for one-thousandth power points as fixers on the second resonance. Original receptance with two resonances plotted as well.*

5.1.2 Subtracting the regeneration

A modified Dobson's analysis was used on the second resonance, of which the results from the sweeper with the highest magnitude were used for a regeneration. This regeneration was then subtracted from the total FRF, in line with Equation (5.1). The result can be seen in Figure 5.8, which shows that the second resonance was clearly decreased in height, resulting in less residual around the frequencies of the first resonance, which is the resonance of interest. A zoom-in of Figure 5.8 can be seen in Figure 5.9.

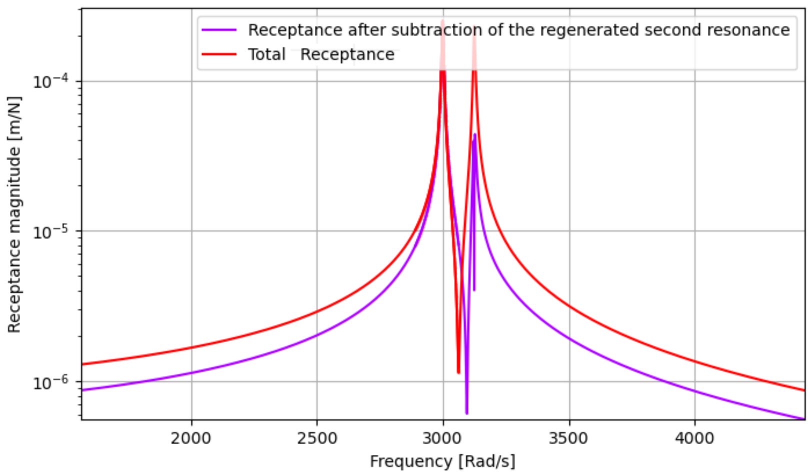

Figure 5.8: *Regenerated second resonance of Figure 5.6 subtracted from the total receptance that also can be seen in Figure 5.6. Total receptance with two resonances plotted for comparison.*

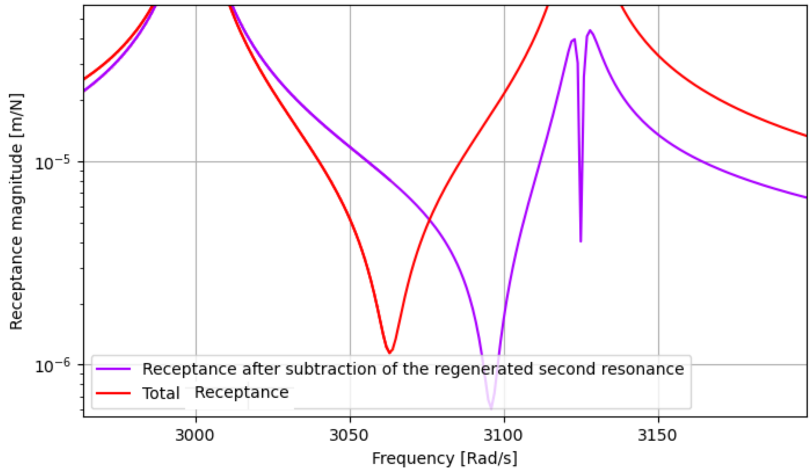

Figure 5.9: *Zoom-in on Figure 5.9 of the second resonance of Figure 5.6 subtracted from the total receptance that also can be seen in Figure 5.6. Total receptance with two resonances plotted for comparison.*

There is a clear dip around 3125 rad/s in the purple line in Figure 5.9, which is caused by the fact that the total receptance and the regeneration that is subtracted to create Figure 5.9 are so close to each other around this frequency, as was seen in Figure 5.7. This creates a very low receptance magnitude value when those are subtracted, but this dip does not affect the residual around the first resonance. Besides this, a larger antiresonance can be seen than in the original receptance, located around 3096 rad/s. This coincides with a crossing frequency of the crossing of the red and blue line in Figure 5.6. Subtracting these complex numbers with a similar receptance magnitude resulting in a very low receptance magnitude value, means that they are (close to) in phase with each other. The reason for the large antiresonance around 3096 rad/s for the purple line in Figure 5.8 and 5.9 is thus that two very similar, in both magnitude and phase, complex numbers are subtracted from each other. This again is a rather local phenomenon, which does not really influence the residual around the first resonance.
It is expected that removal of some of the residual from the second resonance, which is clearly not constant although the (Modified) Dobson's method assumes this, will result in a more accurate Modified Dobson's analysis of the first resonance.

5.1.3 Modified Dobson after subtraction

Subsequently, the Modified Dobson's method using one-thousandth power points fixers is applied to the first resonance, located at 3000 rad/s, of the receptance after subtraction, see the purple line in Figure 5.8 and 5.9.
This resulted in a backbone with less splitting, see the orange line of the Improved Modified Dobson's method in Figure 5.10, in which the comparison is made with the backbone that was seen without any subtraction of a regenerated second mode. The higher receptance magnitude datapoints that are closer to each other result in a less wide top of the backbone peak in this figure. Especially, the left tail of the backbone is much shorter after subtraction, for the right tail not much difference is seen. This results in a smaller standard deviation of the regenerated eigenfrequency for the Improved Modified Dobson's method than without any subtraction of regenerated modes as in Chapter 4, see Table 5.1. Here it can also be seen that the average regeneration eigenfrequency is much closer to the theoretical value of 3000 rad/s for

the case of subtracting the regenerated second mode.
For the modal constants A_r and B_r, the results were also closer to the theoretical values of 2 and 4 kg^{-1} respectively. The damping loss factor η_r is a little more off from the theoretical value of 0.002 than without any subtraction. This was however a special case, as was described in Chapter 4, as one of the tails of the η_r graph became very long for the 125 rad/s distance, which increased the average value massively. The result of this was an average value that was "by coincidence" closer to the theoretical value, but the standard deviation was rather large, as can also be seen in Table 5.1. After subtraction the standard deviation was a lot smaller, resulting in a less wide peak, like for the backbone in Figure 5.10. A similar phenomenon was seen for the modal constants A_r and B_r, which also have smaller standard deviations for the case with subtraction of the regenerated second mode. For the comparison in graphs instead of numbers like in Table 5.1, see Figure 5.11 to 5.13.

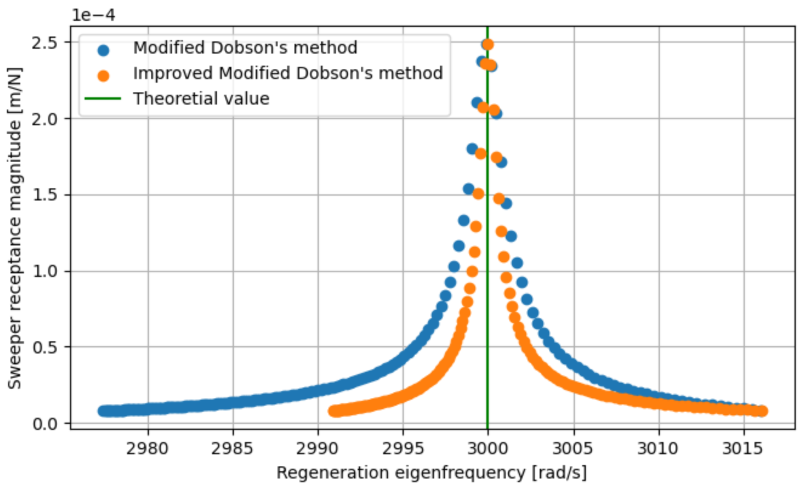

Figure 5.10: *Comparison between the backbone of the first resonance, at 3000 rad/s, with (Improved Modified Dobson's method) and without (Modified Dobson's method) subtraction of the regenerated second peak at 3125 rad/s the theoretical eigenfrequency is depicted by the vertical green line.*

Table 5.1: *Comparison of the modal parameter results coming from the analysis of the first resonance, at 3000 rad/s, with (Improved Modified Dobson's method) and without (Modified Dobson's method) subtraction of the regenerated second peak at 3125 rad/s, all fixers at one-thousandth power points*

Method	Modified Dobson's method	Improved Modified Dobson's method
Average regeneration ω_1 as percentage of theoretical ω_1 [%]	**99.70**	**99.97**
Standard deviation σ of the regeneration ω_1 as percentage of theoretical ω_1 [%]	0.3552	0.2257
Average regeneration η_1 as percentage of theoretical η_1 [%]	**114.15**	**83.85**
Standard deviation σ of the regeneration η_1 as percentage of theoretical η_1 [%]	49.42	10.38
Average regeneration A_1 as percentage of theoretical A_1 [%]	**71.55**	**84.71**
Standard deviation σ of the regeneration A_1 as percentage of theoretical A_1 [%]	10.61	3.388
Average regeneration B_1 as percentage of theoretical B_1 [%]	**81.58**	**85.49**
Standard deviation σ of the regeneration B_1 as percentage of theoretical B_1 [%]	10.92	4.058

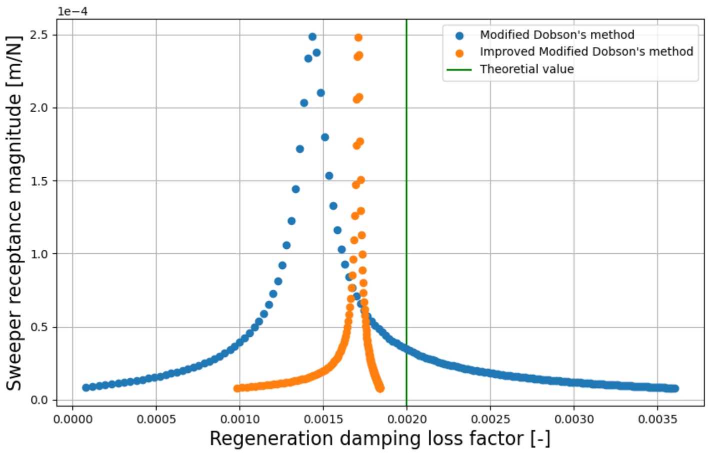

Figure 5.11: *Sweeper receptance magnitude as function of the regenerated damping loss factor η_1 of the first resonance at 3000 rad/s, with (Improved Modified Dobson's method) and without (Modified Dobson's method) subtraction of the regenerated second peak at 3125 rad/s, the theoretical damping loss factor has a value of 0.002 and is depicted by the vertical green line.*

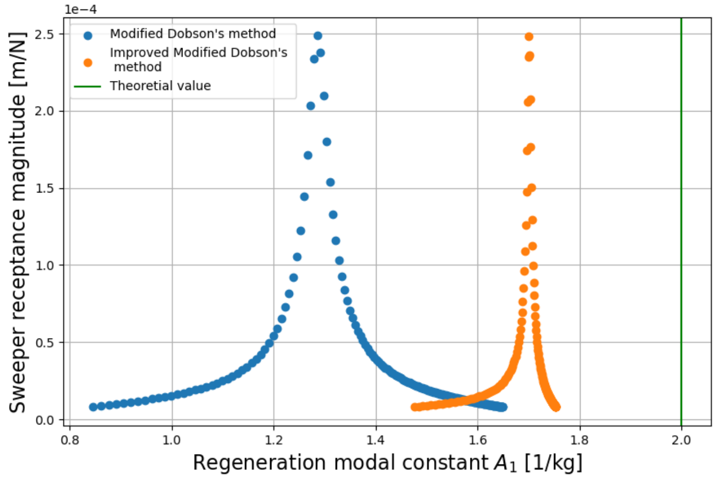

Figure 5.12: *Sweeper receptance magnitude as function of the regenerated modal constant A_1 of the first resonance at 3000 rad/s, with (Improved Modified Dobson's method) and without (Modified Dobson's method) subtraction of the regenerated second peak at 3125 rad/s, the theoretical modal constant A_1 has a value of 2 kg^{-1} and is depicted by the vertical green line.*

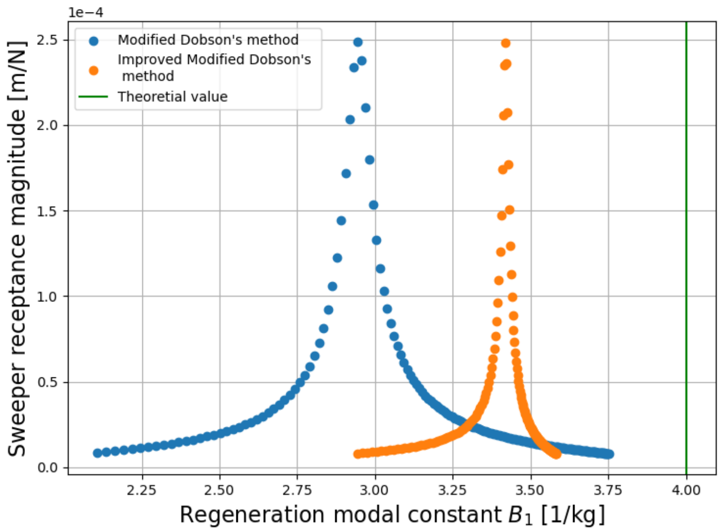

Figure 5.13: *Sweeper receptance magnitude as function of the regenerated modal constant B_1 of the first resonance at 3000 rad/s, with (Improved Modified Dobson's method) and without (Modified Dobson's method) subtraction of the regenerated second peak at 3125 rad/s, the theoretical modal constant B_1 has a value of 4 kg^{-1} and is depicted by the vertical green line.*

5.2 Modified Dobson's method on nonlinear resonances

Besides the linear eigenfrequencies, as are assumed up to this subchapter, there is also the possibility that a system contains nonlinear eigenfrequencies. This subchapter elaborates on those.
For a single nonlinear eigenmode, the Modified Dobson shows a clear backbone, as described in Chapter 4.1. For (non)linear modes that are close to a nonlinear eigenmode of interest, not even as close as bended resonances touching or merging as

discussed earlier, the backbone starts splitting up in tails, like was seen for close linear eigenmodes in Chapter 4.2. This was seen in the analysis of the receptance of two nonlinear resonances in Figure 5.14, of which the first resonance is bended most prominently. The backbone result of the Modified Dobson's analysis [3] for which Di Maio created a computation model is shown in Figure 5.15, where it is compared with the result of the computation model in Python that was created during this project. It can be seen that both computation models show very similar results and taking the average of $\omega_{1,Python}/\omega_{1,DiMaio}$ for each sweeper result gave a difference of only 0.6E-5 %, which is negligible. Similar small differences are seen for the modal parameters η_r, A_r and B_r. The fact that the results are so similar shows that the computation model in Python works correctly.
Other things to notice from these analyses, are that the problem of the splitting of the backbone in Figure 5.15 is seen for nonlinear modes with a close second mode. This clearly shows the limitation of the Modified Dobson's method [3] and the reason to investigate this problem further. Besides this, a clear wobble can be seen at the end of the right tail of the backbone. This is likely caused by the few sweepers that are in between the magnitude heights of the two fixers in Figure 5.14. As the Modified Dobson's method is created for sweepers in between the frequencies of the fixers and above the magnitude of both fixers, sweepers that are not above the magnitude of both fixers can cause disturbances in the results. It is therefore advised to keep the fixers at the same magnitude height as best as possible.
The fixers were put at these locations to make the comparison with the results of the computation model of Di Maio as fair as possible. They are not close to the one-thousandth power points, as those would be located below the magnitude level of the anti-resonance around 665 Hz. In such a case, higher fixer locations are needed, as the anti-resonance would also not count as the linear regime for the location of the fixers for a nonlinear eigenfrequency. The locations in Figure 5.14 seem about right for that, especially as the left fixers could not be placed at a much lower frequency. Equal magnitude height for the fixers would be preferred, though.

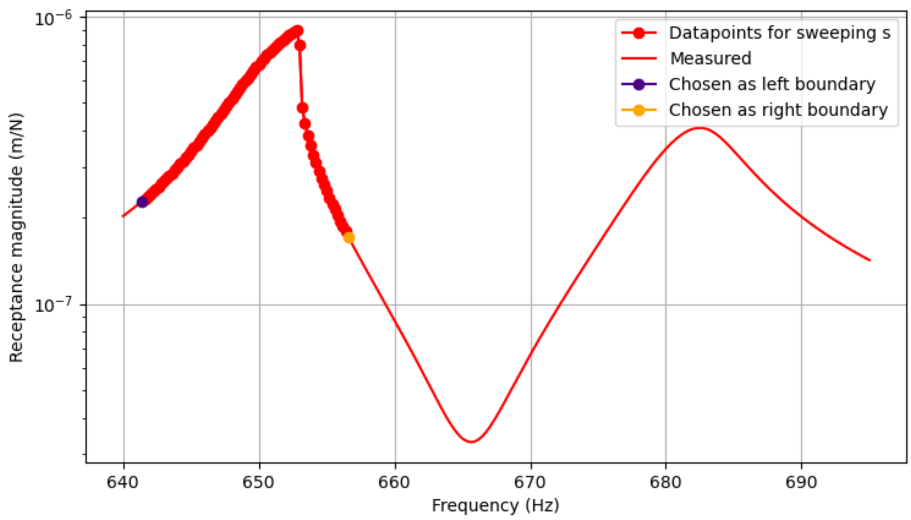

Figure 5.14: *Fixer locations for analysing the first nonlinear resonance of a receptance with two resonances, "s" stand for sweeper-point here and "Measured" means datapoints that are not used in the analysis and are therefore plotted as a line, 1 Hz = 2 π rad/s.*

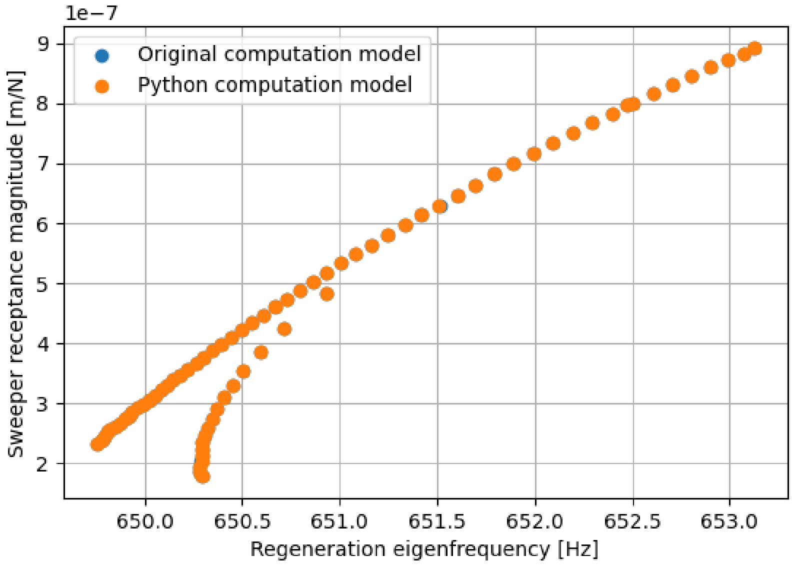

Figure 5.15: *Backbone of the first resonance of Figure 5.14 for the fixer locations in that figure, for both the analyses of the computation model from Di Maio and the newly created in Python*

It is expected that the Improved Modified Dobson's method also helps to reduce this splitting of the backbone of a skewed nonlinear resonance with a close linear resonance. Testing this was, however, not possible, as the second mode in Figure 5.14 is also a nonlinear resonance and can therefore not be regenerated and subtracted easily. The bending of the backbone of the second resonance, which is a sign of nonlinearity, can be seen in Figure 5.16. Here the splitting of the backbone is seen for the full graph, which is likely caused by the fact that the residual-curve of the first mode is rather steep, as this mode has a much higher magnitude. The residual-curve of the second mode, at the frequency range between the fixers of the first mode in Figure 5.14, is probably much less steep and thus closer to a constant residual situation, causing less splitting of the backbone of the first mode.

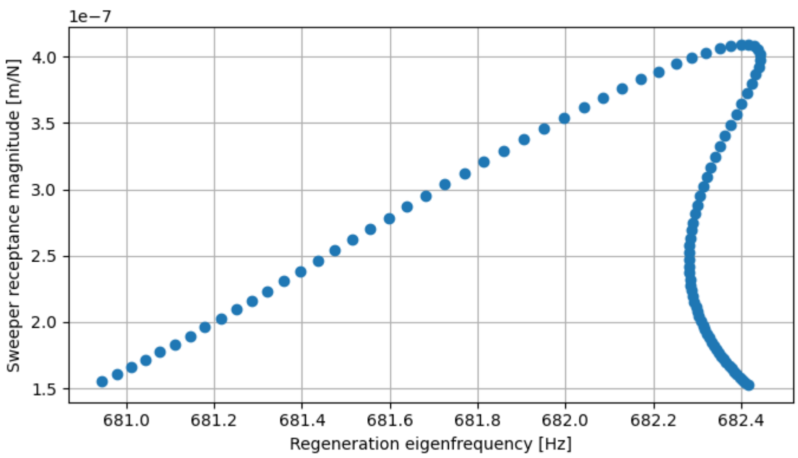

Figure 5.16: *Backbone of the second resonance of Figure 5.14 for the fixer locations as low as possible to have them at the linear regime.*

Removing the residuals coming from other nonlinear resonance could be possible by fitting a linear resonance that fits at the linear regime of the nonlinear resonance. This way the skewed top of the resonance is not fitted, but this part does not need to be regenerated and subtracted per se. As long as the fit at the linear regime is satisfactory, the residual further away from the resonance, at the frequency range of another resonance that is of interest, can be approximated closely. This regeneration can then be subtracted from the total receptance, like was described in Chapter 5.1.2. This new total receptance can then be used to do the Modified Dobson's analysis of the first nonlinear resonance, which will likely regenerate less splitting of the backbone.

5.3 Conclusion

It is expected that making the curve of the residual from other modes less steep, by subtracting a regeneration of the mode that is the source of this residual, will result in less effect of this residual on the Modified Dobson's method. This method assumes a constant residual and a less steep residual curve is closer to a constant residual situation than a very steep residual curve. The residual from other modes is expected to cause problem for both linear systems, that were analysed here, and nonlinear systems. An Improved Modified Dobson's method was described: the subtraction of a regenerated second resonance from the total receptance resulted in a more accurate Modified Dobson's analysis of the first resonance. This was seen for the 125 rad/s distance between the resonances case described in this chapter, but is expected to work for other distances between the resonance cases from Chapter 4 as well. The Improved Modified Dobson's method results are still not a smooth and clean backbone, but the results get closer to such a backbone. Iterating the process of analysing one resonance, to decrease its residual-effect on the other resonance by subtraction, could be an option to get closer to a clear backbone. By doing this from resonance 2 to resonance 1, then from 1 to 2 and back from resonance 2 to 1 again, possibly more favourable results are seen.

For the analysis of the second resonance of a linear system, of which the results are used for the subtraction, the Modified Dobson's method was used. Then the highest magnitude sweeper result was picked for the regeneration, as this showed favourable results over other sweepers. Other analysis methods might be possible here, especially in the case of a linear mode, to have a more accurate regeneration of the second resonance. The Dobson's method for instance, take many more datapoints into account than just the three points that are used for a single regeneration in the Modified Dobson's method, which will improve the accuracy. This would result in a cleaner subtraction. For the Improved Modified Dobson's method, already improvements were seen using this not very accurate regeneration for subtraction. It is expected that more accurate regeneration will result in more favourable results. Some iteration as described earlier could also help to increase the accuracy of the regeneration.

The Python computational model created during this thesis correctly models the Modified Dobson's method, as shows the comparison of the results of both this and the computational modal created by Di Maio.
For the Modified Dobson's method, it is important to have the fixers at close magnitude levels and to have them in the linear regime of the resonance of interest.
A splitting of the backbone in case of close other modes was seen for nonlinear resonances, just like this was seen for linear resonances.
A resonance with a higher magnitude level will likely cause more splitting of backbones of other modes, as its residual-curve is more steep, causing more problems for the Modified Dobson's method.

It is expected that the Improved Modified Dobson's method also helps to reduce this splitting of the backbone of a skewed nonlinear resonance with a close linear resonance.
For a close skewed resonance to the skewed resonance, fitting a linear resonance to the linear regime of a skewed nonlinear resonance could be a way to approximate this residual-curve and then remove it by subtracting this fitted linear resonance. This could reduce the splitting of the backbone in case of two skewed resonances.

6 Conclusions and recommendations

6.1 Conclusions

The first part of the research question to be answered is:

What is the effect of an increasingly closer other mode on the Modified Dobson's analysis of the mode of interest?

It can be concluded that the lists of each modal parameter, η_r, A_r, B_r, including the list of eigenfrequency ω_r, that are found for a linear resonance with the Modified Dobson's method become increasingly less accurate for a decrease in the distance between resonances. This means that, for example, the backbone is shifted towards a frequency that is not the eigenfrequency of the resonance. Besides this, the spread of the regenerated modal parameters increases, which makes that, for instance, the backbone starts splitting and becomes less distinct.
The maximum IMC value to see minimal interference between the resonances turns out to be much lower for the Modified Dobson's method compared to the line-fit method that the IMC was designed for by Maia [22], which indicates that the Modified Dobson's method is sensitive to close other modes.
Besides the distance between the resonances, also the damping of the resonances is of influence on the IMC. According to the theory of the IMC, it increases for a higher damping of both resonances while keeping the ratio between the two constant, so more distance between the resonances is needed in that case to stay below the maximum IMC value

The second part of the research question is:

How can negative effects of a close mode be reduced, to improve the results of the Modified Dobson's method?

It is expected that making the curve of the residual from other modes less steep, by subtracting a regeneration of the mode that is the source of this residual, will result in less effect of this residual on the Modified Dobson's method. This method assumes a constant residual and a less steep residual curve is closer to a constant residual situation than a very steep residual curve. The residual from other modes is expected to cause problem for both linear systems, that were analysed here, and nonlinear systems. An Improved Modified Dobson's method was described: the subtraction of a regenerated second resonance from the total receptance resulted in a more accurate Modified Dobson's analysis of the first resonance. This was seen for the 125 rad/s distance between the resonances case described in this chapter, but is expected to work for other distances between the resonance cases from Chapter 4 as well. The Improved Modified Dobson's method results are still not a smooth and clean backbone, but the results get closer to such a backbone. Iterating the process of analysing one resonance, to decrease its residual-effect on the other resonance by subtraction, could be an option to get closer to a clear backbone. By doing this from resonance 2 to resonance 1, then from 1 to 2 and back from resonance 2 to 1 again, possibly more favourable results are seen.

For the analysis of the second resonance of a linear system, of which the results are used for the subtraction, the Modified Dobson's method was used. Then the highest magnitude sweeper result was picked for the regeneration, as this showed favourable results over other sweepers. Other analysis methods might be possible here, especially in the case of a linear mode, to have a more accurate regeneration of the second resonance. This would result in a cleaner subtraction. For the Improved Modified Dobson's method, already improvements were seen using this not very accurate regeneration for subtraction. It is expected that more accurate regeneration will result in more favourable results. Some iteration as described earlier could also help to increase the accuracy of the regeneration.

It is expected that the Improved Modified Dobson's method also helps to reduce this splitting of the backbone of a skewed nonlinear resonance with a close linear resonance.
For a close skewed resonance to the skewed resonance, fitting a linear resonance to the linear regime of a skewed nonlinear resonance could be a way to approximate this residual-curve and then remove it by subtracting this fitted linear resonance. This could reduce the splitting of the backbone in case of two skewed resonances.

Other conclusions that can be drawn are:

- The Python computational model created during this thesis correctly models the Modified Dobson's method, as shows the comparison of the results of both this computational model and the computational model of Di Maio.
- For the Modified Dobson's method, it is important to have the fixers at close magnitude levels, to avoid wobbles in the backbone graph, and to have them in the linear regime of a skewed resonance of interest.
- A splitting of the backbone in case of close other modes was seen for nonlinear resonances, just like this was seen for linear resonances.
- A resonance with a higher magnitude level will likely cause more splitting of backbones of other modes, as its residual-curve is more steep, causing more problems for the Modified Dobson's method.

6.2 Recommendations

- Try to reduce the splitting of a backbone of skewed resonance that is close to a resonance of a linear mode. This way the Improved Modified Dobson's method can be tested for a skewed resonance. item Fitting a linear resonance to the linear regime of a nonlinear resonance might be a way to approximate this residual-curve and then remove it by subtracting this fitted linear resonance. This could reduce the amount of splitting of the backbone of resonances close to this nonlinear resonance, as the residual of it could be closer to constant then.
- Look into difference between taking fixers at as much the same height as possible or try them both to be as close to the prescribed one-thousandth point (or other point) as possible. In the end this might lead to a more fair comparison between distance of close modes, but the latter option can result in a sweeper in between the fixers in magnitude, which could give strange results for that sweeper, like was in Chapter 5.2.
- More research would be needed to determine the maximum IMC value more precisely for the Modified Dobson's method.
- The IMC in Chapter 4 is calculated using the theoretical modal parameter values, for an experiment this is less easy, so it is recommended to search for a

way to extract one set of the four modal parameters from the Modified Dobson's method that is usable for this, especially in the case of nonlinear eigenfrequencies.

- The requirement of the Ω to be close to ω_r for the Modified Dobson's method might conflict with the fixers located at the linear-regime of a nonlinear resonance, as the fixers might be rather far apart from each other then. This will result in Ω values for the fixers and the sweeper that are not close to the eigenfrequency ω_r. More information about the exact reason for the failing of the Modified Dobson's method might be found in this direction.

References

[1] D. J. Ewins. *Modal Testing: Theory, Practice and Application*. Research Studies Press, 2000.

[2] K. Worden and G. Tomlinson. *Nonlinearity in Structural Dynamics: Detection, Identification and Modeling*. Institute of Physics, 2001.

[3] D. Di Maio. A novel analysis method for calculating nonlinear frequency response functions. Journal of Structural Dynamics 3 (2025) 30-57. https://doi.org/10.25518/2684-6500.242.

[4] N. M. M. Maia and J. M. M. Silva. *Theoretical and Experimental Modal Analysis*. Research Studies Press, 1997.

[5] A. Nayfeh and D. Mook. *Nonlinear Oscillations*. Wiley, 1995.

[6] T. Karaağaçlı and H. N. Özgüven. Experimental modal analysis of nonlinear systems by using response-controlled stepped-sine testing. Mechanical Systems and Signal Processing 146 (2021) 107023. https://doi.org/10.1016/j.ymssp.2020.107023.

[7] G. Abeloos; L. Renson; C. Collette and G. Kerschen. Stepped and swept control-based continuation using adaptive filtering. Nonlinear Dynamics 104 (2021) 3793–3808. https://doi.org/10.1007/S11071-021-06506-Z.

[8] M. Li; S. Jain and G. Haller. Fast computation and characterization of forced response surfaces via spectral submanifolds and parameter continuation. Nonlinear Dynamics 112 (2024) 7771–7797. https://doi.org/10.1007/S11071-024-09482-2.

[9] R. Rosenberg. On nonlinear vibrations of systems with many degrees of freedom. Advances in Applied Mechanics 9 (1966) 155–242. https://doi.org/10.1016/S0065-2156(08)70008-5.

[10] M. Peeters; G. Kerschen and J. C. Golinval. Dynamic testing of nonlinear vibrating structures using nonlinear normal modes. Journal of Sound and Vibration 330 (2011) 486–509. https://doi.org/10.1016/J.JSV.2010.08.028.

[11] S. Peter and R. I. Leine. Excitation power quantities in phase resonance testing of nonlinear systems with phase-locked-loop excitation. Mechanical Systems and Signal Processing 96 (2017) 139–158. https://doi.org/10.1016/J.YMSSP.2017.04.011.

[12] L. Renson; A. Gonzalez-Buelga; D. A. Barton and S. A. Neild. Robust identification of backbone curves using control-based continuation. Journal of Sound and Vibration 367 (2016) 145 158. https://doi.org/10.1016/J.JSV.2015.12.035.

[13] T. Karaağaçlı and H. N. Özgüven. Experimental identification of backbone curves of strongly nonlinear systems by using response-controlled stepped-sine testing (rct). Vibration 3 (2020) 266–280. https://doi.org/10.3390/vibration3030019.

[14] T. Karaağaçlı and H. N. Özgüven. Experimental quantification and validation of modal proper ties of geometrically nonlinear structures by using response-controlled stepped-sine testing. Experimental Mechanics 62 (2022) 199–211. https://doi.org/10.1007/s11340-021-00784-9.

[15] G. Zhang; C. Zang and M. I. Friswell. Identification of weak nonlinearities in mdof systems based on reconstructed constant response tests. Archive of Applied Mechanics 89 (2019) 2053–2074. https://doi.org/10.1007/s00419-019-01559-4.

[16] G. Zhang; C. Zang and M. I. Friswell. Measurement of multivalued response curves of a strongly nonlinear system by exploiting exciter dynamics. Mechanical Systems and Signal Processing 140 (2020) 106474. https://doi.org/10.1016/j.ymssp.2019.106474.

[17] G. Zhang; C. Zang and M. I. Friswell. Measurement of the multivalued phase curves of a strongly nonlinear system by fixed frequency tests. Archive of Applied Mechanics 90 (2020) 2543–2560. https://doi.org/10.1007/S00419-020-01736-W.

[18] A. Carrella and D. J. Ewins. Identifying and quantifying structural nonlinearities in engineering applications from measured frequency response functions. Mechanical Systems and Signal Processing 25 (2011) 1011–1027. https://doi.org/10.1016/j.ymssp.2010.09.011.

[19] A. Carrella. Nonlinear identifications using transmissibility: Dynamic characterisation of anti vibration mounts (avms) with standard approach and nonlinear analysis. International Journal of Mechanical Sciences 63 (2012) 74–85. https://doi.org/10.1016/j.ijmecsci.2012.06.014.

[20] R. Lin. Identification of the dynamic characteristics of nonlinear structures. Ph.D. thesis, Imperial College London (1990).

[21] B. J. Dobson. A straight-line technique for extracting modal properties from frequency response data. Mechanical Systems and Signal Processing 1 (1987) 29–40. https://doi.org/10.1016/0888-3270(87)90081-1.

[22] N. M. M. Maia. Extraction of valid modal properties from measured data in structural vibration. Ph.D. thesis, Imperial College London (1988).

[23] N. M. M. Maia. A global version of dobson's method. In Proceeding of the International Modal Analysis Conference (1992) 907-911.

[24] R. E. D. Bishop. The general theory of "hysteretic damping". Aeronautical Quarterly Volume 7 Issue 1 (1956) 60-70. https://doi.org/10.1017/S0001925900010131.

[25] B. J. Dobson. Modal analysis using dynamic stiffness data. Royal Naval Engi neering College (RNEC) (1984) TR-84015.

A Appendix

A.1 Nyquist circle of an SDOF linear system with hysteretic damping

From Equation (3.7) it follows that

$$\alpha(\omega) = \mathrm{Re}(\alpha(\omega)) + i\mathrm{Im}(\alpha(\omega)), \tag{A.1}$$

with

$$\mathrm{Re}(\alpha(\omega)) = \frac{k - \omega^2 m}{(k - \omega^2 m)^2 + d^2}, \tag{A.2}$$

and

$$\mathrm{Im}(\alpha(\omega)) = \frac{-d}{(k - \omega^2 m)^2 + d^2}. \tag{A.3}$$

From knowing that

$$[\mathrm{Re}(\alpha(\omega))^2 + \mathrm{Im}(\alpha(\omega))^2] - [\mathrm{Re}(\alpha(\omega))^2 + \mathrm{Im}(\alpha(\omega))^2] = 0, \tag{A.4}$$

it can be obtained that

$$[\mathrm{Re}(\alpha(\omega))^2 + \mathrm{Im}(\alpha(\omega))^2] - \frac{1}{(k - \omega^2 m)^2 + d^2} = 0, \tag{A.5}$$

which can be rewritten to

$$\mathrm{Re}(\alpha(\omega))^2 + [\mathrm{Im}(\alpha(\omega)) + \frac{1}{2d}]^2 = [\frac{1}{2d}]^2. \tag{A.6}$$

This is clearly the form of the equation of a circle, with $\frac{1}{2d}$ being radius of the circle.

A.2 Line-fit method formulas

The full description of the line-fit parameters is:

$$m_R = \frac{(A_r + B_r \eta_r)\omega_r^2}{A_r^2 + B_r^2} \tag{A.7}$$

$$m_I = \frac{(A_r \eta_r - B_r)\omega_r^2}{A_r^2 + B_r^2} \tag{A.8}$$

$$n_R = -\frac{A_r}{A_r^2 + B_r^2} \tag{A.9}$$

$$n_I = \frac{B_r}{A_r^2 + B_r^2} \tag{A.10}$$

A.3 Maximum receptance magnitude for regeneration

When a certain mode is regenerated using Equation 3.9, the maximum receptance magnitude of the resoance can be calculated as follows:
At the maximum, it holds that $\omega = \omega_r$, which results in:

$$\alpha_r = \frac{A_r + iB_r}{i\eta_r \omega_r^2} \tag{A.11}$$

Multiplying the numerator and denominator with -i and taking the magnitude gives:

$$|\alpha_r|_{\max} = |\frac{1}{\eta_r\omega_r^2}| \cdot |B_r - iA_r| \tag{A.12}$$

$$= |\frac{1}{\eta_r\omega_r^2}| \cdot \sqrt{A_r^2 + B_r^2} \tag{A.13}$$

This means that the maximum receptance magnitude is inversely proportional to the structural damping factor of that mode, η_r, and inversely squared proportional to the eigenfrequency ω_r. In case A and B are both doubled, the maximum of the resonance magnitude doubles as well. However, the effect of just doubling A is not as straightforward.

A.4 Interference phase criterion

The IPC [22] for the phase interference of mode 2 on mode 1 is

$$\frac{2\delta a^4\gamma}{[(\frac{1-a^2}{\eta_1})^2 + \gamma^2 - a^4]\sqrt{(\frac{1-a^2}{\eta_1})^2 + \gamma^2}} \leq \nu_{phase}, \tag{A.14}$$

in which the same definitions of a, γ and δ as in Equation (3.39) apply. This criterion does not have a limit value for ν_{phase} but the phase criteria could be compared to each other to see which combination of modes has more phase interference than the other.
Like for the interference magnitude criterion, an increase in a, as well as an increase in δ or η_1 (while keeping γ constant) or both result in an increase of the interference phase criterion value, so in both magnitude and phase more interference is seen in these cases. An increase in damping ratio γ however, leads to a decrease of the interference phase criterion, except for low values of η_1, order 0.001, where a small increase of the phase criterion was seen in [22]. This is different for the interference magnitude criterion which is barely affected by a change in γ.

A.5 Modified Dobson's method close modes mathematics

In case of a linear relation between residual and frequency, Equations 3.14 and 3.21 become

$$\alpha(\omega) = \frac{A_r + iB_r}{\omega_r^2 - \omega^2 + i\eta_r\omega_r^2} + (p + iq)\omega, \tag{A.15}$$

$$\alpha(\Omega) = \frac{A_r + iB_r}{\omega_r^2 - \Omega^2 + i\eta_r\omega_r^2} + (p + iq)\Omega. \tag{A.16}$$

Which means that Equation 3.23 becomes the rather complicated

$$\Lambda = \frac{\omega^2 - \Omega^2}{\frac{(A_r+iB_r)(\omega^2-\Omega^2)}{(\omega_r^2-\omega^2)(\omega_r^2-\Omega^2)-\eta_r^2\omega_r^4+i\eta_r\omega_r^2(2\omega_r^2-\omega^2-\Omega^2)} + (p+iq)(\omega - \Omega)} \tag{A.17}$$

$$= \frac{\omega + \Omega}{\frac{(A_r+iB_r)(\omega+\Omega)}{(\omega_r^2-\omega^2)(\omega_r^2-\Omega^2)-\eta_r^2\omega_r^4+i\eta_r\omega_r^2(2\omega_r^2-\omega^2-\Omega^2)} + (p+iq)}. \tag{A.18}$$

In case of a quadratic relation between residual and frequency this is even more complicated with

$$\Lambda = \frac{\omega^2 - \Omega^2}{\frac{(A_r+iB_r)(\omega^2-\Omega^2)}{(\omega_r^2-\omega^2)(\omega_r^2-\Omega^2)-\eta_r^2\omega_r^4+i\eta_r\omega_r^2(2\omega_r^2-\omega^2-\Omega^2)} + (p+iq)(\omega^2 - \Omega^2)} \tag{A.19}$$

$$= \frac{(\omega_r^2-\omega^2)(\omega_r^2-\Omega^2)-\eta_r^2\omega_r^4+i\eta_r\omega_r^2(2\omega_r^2-\omega^2-\Omega^2)}{(A_r+iB_r)+((\omega_r^2-\omega^2)(\omega_r^2-\Omega^2)-\eta_r^2\omega_r^4+i\eta_r\omega_r^2(2\omega_r^2-\omega^2-\Omega^2))(p+iq)}. \tag{A.20}$$

The full equations, without any assumed relationships for the residuals become

$$\alpha(\omega) = \frac{A_r+iB_r}{\omega_r^2-\omega^2+i\eta_r\omega_r^2} + \frac{A_{r2}+iB_{r2}}{\omega_{r2}^2-\omega^2+i\eta_{r2}\omega_{r2}^2}, \tag{A.21}$$

$$\alpha(\Omega) = \frac{A_r+iB_r}{\omega_r^2-\Omega^2+i\eta_r\omega_r^2} + \frac{A_{r2}+iB_{r2}}{\omega_{r2}^2-\Omega^2+i\eta_{r2}\omega_{r2}^2} \tag{A.22}$$

and

$$\Lambda = \frac{1}{\frac{A_r+iB_r}{(\omega_r^2-\omega^2)(\omega_r^2-\Omega^2)-\eta_r^2\omega_r^4+i\eta_r\omega_r^2(2\omega_r^2-\omega^2-\Omega^2)} + \frac{A_{r2}+iB_{r2}}{(\omega_{r2}^2-\omega^2)(\omega_{r2}^2-\Omega^2)-\eta_{r2}^2\omega_{r2}^4+i\eta_{r2}\omega_{r2}^2(2\omega_{r2}^2-\omega^2-\Omega^2)}}. \tag{A.23}$$

A.6 Global Dobson's method

One way of analysing these multiple FRF's from a SIMO experiment is the Global Dobson's method [23]. It is based on the Dobson's method as described in Chapter 3.4.3, but now the Dobson's parameters, Equations 3.30 to 3.33, are calculated for each each FRF instead of for only one. This will regenerate 4 Dobson's parameter per FRF for a peak in a certain frequency range, which are then used to calculate the eigenfrequency of the systen with

$$\omega_{r,G}^2 = \frac{\sum_{i=1}^{p}(-d_R u_R - d_I u_I)_i}{\sum_{i=1}^{p}(u_R^2 + u_I^2)_i}, \tag{A.24}$$

in which r is the eigenmode that is investigate, G stands for Global Dobson and p is the amount of FRF's that are taken into account. Similarly, the damping is calculated using

$$\eta_{r,G} = \frac{\sum_{i=1}^{p}(d_R u_I - d_I u_R)_i}{\sum_{i=1}^{p}(-d_R u_R - d_I u_I)_i}, \tag{A.25}$$

where p is again the amount of FRF's. Note the similarity between Equation A.24 and A.25 and from Chapter 3.4.3, Equation 3.34 and 3.35 respectively.

The calculation of the modal constants for the Global Dobson's method is a little less straightforward. It starts with the local Dobson's parameters as used in Equation A.24 and A.25 and local damping values, η_{ri}, calculated using Equation 3.35. These are then (pre)multiplied with the Global values from Equation A.24 and A.25. This gives

$$\begin{Bmatrix} d_{R,G} \\ d_{I,G} \end{Bmatrix}_{ri} = \begin{bmatrix} -\omega_{r,G}^2 & \eta_{r,G}\omega_{r,G}^2 \\ -\eta_{r,G}\omega_{r,G}^2 & -\omega_{r,G}^2 \end{bmatrix} \begin{Bmatrix} u_R \\ u_I \end{Bmatrix}_{ri}, \tag{A.26}$$

and

$$\begin{Bmatrix} u_{R,G} \\ u_{I,G} \end{Bmatrix}_{ri} = \frac{1}{\omega_{r,G}^2(\eta_{r,G}^2 - 1)} \begin{bmatrix} 1 & \eta_{ri} \\ -\eta_{ri} & 1 \end{bmatrix} \begin{Bmatrix} d_R \\ d_I \end{Bmatrix}_{ri}, \tag{A.27}$$

where the G stands again for Global, but in the case of the 4 Global Dobson's parameters calculated here, they are calculated per FRF. This, in contrary to the Global values calculated in Equation A.24 and A.25, which are for the total experiment. The i in Equation A.26 and A.27 is the number of the FRF, so i will run from 1 to p, with p being the total number of FRF's that are generated during the experiment. The letter r is for the number of the eigenmode that is being investigated.
For each set of Global Dobson's parameters the Global modal parameters, $A_{r,G}$ and $B_{r,G}$ of that FRF can be calculated. This is done using Equation 3.36 and 3.37, but then with Global instead of normal Dobson's parameters.
In contrary to the Dobson's method, the Global Dobson's method will thus generate multiple modal constants A_r and B_r, one set for each FRF, as there are also multiple FRF's measured, which is not the case for the Dobson's method. The Global modal parameters $A_{r,G}$ and $B_{r,G}$ that are calculated are related to a certain measurement point, where the acceleration, velocity or displacement is measured, which is used to generate the FRF for that location.
When the measurement point is at the same location as where the excitation force is introduced to the system, this will generate a drive-point FRF. The measurement point could also be on the direct opposite side of the excitation point for a thin structure, where the direction of measurement needs to be noted carefully to prevent plus-minus-mistakes, then it is still considered a drive-point FRF.
When the measurement point is at another location than the excitation point, it will

generate a transfer FRF, as the force will transfer through the structure and result in a certain response at the measurement point.
The drive-point and transfer FRF's will thus all have Global modal constants $A_{r,G}$ and $B_{r,G}$ which can be used to plot modes of the structure, as a vector that can be drawn for each modal constants pair is located at the measurement point of the structure. For instance, 5 FRF's are being creating using 5 measurement points on the structure, thus a mode shape consisting of 5 points in space can be generated.

Possible Global Modified Dobson's method

The initial goal of this thesis was to program a Global Modified Dobson's method in Python. During the process, it was, however, found that the sensitivity of the Modified Dobson's method needed to be solved first. As the method by nature is very sensitive to close other modes, it does not make sense to program this for multiple FRF's, as complex structures that needed multiple sensors in general contain a lot of (close) modes.

Besides the failure of the Modified Dobson for close modes, there are some more difficulties in extending this method to Global, compared to the extension of the "classical" Dobson's method to the Global one. The Modified Dobson's method finds an eigenfrequency value for every single sweeper point of the peak, compared to just one eigenfrequency value per peak. Equation A.24 could then be used once for every single sweeper point to find an $\omega_{r,G}$ value per sweeper, with the requirement that the frequency of the sweeper is equal in all the different FRF's. An equal sampling frequency for generating the FRF from each measurement point is thus needed. A similar procedure could be followed for the Global damping value $\eta_{r,G}$ of each sweeper point, see Equation A.25.
The 4 Global Modified Dobson's parameters are then calculated using

$$\begin{Bmatrix} d_{R,G} \\ d_{I,G} \end{Bmatrix}_{rij} = \begin{bmatrix} -\omega_{r,Gj}^2 & \eta_{r,Gj}\omega_{r,Gj}^2 \\ -\eta_{r,Gj}\omega_{r,Gj}^2 & -\omega_{r,Gj}^2 \end{bmatrix} \begin{Bmatrix} u_R \\ u_I \end{Bmatrix}_{rij}, \tag{A.28}$$

and

$$\begin{Bmatrix} u_{R,G} \\ u_{I,G} \end{Bmatrix}_{rij} = \frac{1}{\omega_{r,Gj}^2(\eta_{r,Gj}^2 - 1)} \begin{bmatrix} 1 & \eta_{rij} \\ -\eta_{rij} & 1 \end{bmatrix} \begin{Bmatrix} d_R \\ d_I \end{Bmatrix}_{rij}, \tag{A.29}$$

in which r is the number of the eigenmode, i is the number of the FRF and j is the number of the sweeper point. This leads, per eigenmode, to $i \cdot j$ sets of 4 Global Modified Dobson's parameters and thus also $i \cdot j$ sets of modal constants $A_{r,G}$ and $B_{r,G}$. The size of the analysis results will thus increase largely with this method compared to the Global Dobson's method. Especially, to give some size indication, as the amount of sweeper points in general will be larger than the amount of FRF's that are taken into account.